PROOF COVER SHEET

Journal acronym:	TRES
Author(s):	A. Kokhanovsky, V. V. Rozanov, T. Aoki, D. Odermatt, C. Brockmann, O. Krüger, M. Bouvet, M. Drusch and M. Hori
Article title:	Sizing snow grains using backscattered solar light
Article no:	560621
Enclosures:	1) Query sheet 2) Article proofs

Dear Author,

1. Please check these proofs carefully. It is the responsibility of the corresponding author to check these and approve or amend them. A second proof is not normally provided. Taylor & Francis cannot be held responsible for uncorrected errors, even if introduced during the production process. Once your corrections have been added to the article, it will be considered ready for publication.

For detailed guidance on how to check your proofs, please see http://journalauthors.tandf.co.uk/production/checkingproofs.asp.

2. Please review the table of contributors below and confirm that the first and last names are structured correctly and that the authors are listed in the correct order of contribution. This check is to ensure that your name will appear correctly online and when the article is indexed.

Sequence	Prefix	Given name(s)	Surname	Suffix
1		A.	Kokhanovsky	
2		V. V.	Rozanov	
3		T.	Aoki	
4		D.	Odermatt	
5		C.	Brockmann	
6		O.	Krüger	
7		M.	Bouvet	
8		M.	Drusch	
9		M.	Hori	

Queries are marked in the margins of the proofs. Unless advised otherwise, submit all corrections and answers to the queries using the CATS online correction form, and then press the "Submit All Corrections" button.

AUTHOR QUERIES

General query: You have warranted that you have secured the necessary written permission from the appropriate copyright owner for the reproduction of any text, illustration, or other material in your article. (Please see http://journalauthors.tandf.co.uk/preparation/permission.asp.) Please check that any required acknowledgements have been included to reflect this.

AQ1 Please provide full and complete affiliations for all authors.

AQ2 Please check that 'μm' is correct in '1240 μm'.

AQ3 References Massom *et al*. 2001, Kokhanovsky *et al*. 2005, Peltoniemi 2007, Khokhanovsky 2006 and Spagenberg *et al.* 2001 are cited in the text, but not given in the References list. Please provide full references, or delete the text citations.

AQ4 Please define '*n*' and 'χ'.

AQ5 Please define 'SGS'.

AQ6 Please check the equation numbers in 'equation (38) (see also equations (9) and (41))'.

AQ7 Please check the equation number in 'equation (21)'.

AQ8 The dates in tables 2 and 3 have been changed to journal style, please check.

AQ9 Please provide geographical coordinates and a distance scale bar for figure 11.

AQ10 Please correct the citation to figure 36.

AQ11 Please check the sentence beginning 'The presence of liquid films. . .'.

AQ12 References Dozier and Painter 2004, Hansen and Nazernko 2004, Kokhanovsky *et al.* 2007 and Tomasi *et al.* 2007 are given in the References list, but not cited in the text. Please insert text citations, or delete these references from the list.

AQ13 Please update publication details for reference Zuravleva and Kokhanovsky 2011 submitted.

AQ14 Please provide higher resolution versions (at least 600 dpi) of all figures, ensuring that all parameters and symbols match and are fully consistent with those in the text (e.g. if they are italic in the text, please make them italic in the figures). In addition, please label figure part numbers as '(*a*)', '(*b*)', etc.; use '°' instead of 'degrees'; use an initial capital letter only for the first word of all axes labels, and put units in brackets (e.g.'(°)') at the end of axes labels; change numbers such as '10000' to '10 000'; and put the units in figure 14 in the format 'ng g^{-1}'.

TRES_A_560621

International Journal of Remote Sensing
Vol. 00, No. 00, Xxxx 2011, 1–33

Taylor & Francis
Taylor & Francis Group

Sizing snow grains using backscattered solar light

A. KOKHANOVSKY†, V. V. ROZANOV†, T. AOKI‡, D. ODERMATT§,
C. BROCKMANN¶, O. KRÜGER¶, M. BOUVET|, M. DRUSCH| and M. HORI¤

†Institute of Environmental Physics, University of Bremen, Germany
‡Meteorological Research Institute, Tsukuba, Japan
§University of Zurich, Switzerland
¶Brockmann Consult, Geesthacht, Germany
|European Space Agency, Noordwijk, The Netherlands
¤Japan Aerospace Exploration Agency, Tokyo, Japan

(*Received 6 January 2010; in final form 23 July 2010*)

In this paper, we describe a technique to determine dry snow grain size from optical observations. The method is based on analysis of the snow reflectance in the near-infrared region, in particular, the Medium Resolution Imaging Spectrometer (MERIS) band at 865 nm, which is common to many spaceborne optical sensors, is used. In addition, the algorithm is applied to the Moderate Resolution Imaging Spectroradiometer (MODIS) 1240 nm band. A sensitivity study is performed, and it is shown that the bands are superior with respect to information content, as far as snow grain size remote sensing is concerned. It is found that bands located at 1020 and 1240 μm are the most suitable for snow grain size remote-sensing applications. The developed method is validated using MODIS observations over flat snow deposited on a lake ice in Hokkaido, Japan.

1. Introduction

Understanding global physical properties of snow and also trends in snow cover and pollution is of a great importance for a number of disciplines that include climate studies, environmental physics and snow hydrology (Dozier 1987, Massom *et al.* 2001). In this paper, we address a question of subsurface snow grain size monitoring using optical measurements. It is known that the snow grain size determines the level of light absorbance by snow and that this parameter is needed to assess the heat balance in snow and also the timing and magnitude of snowmelt.

The first question, which is important to answer in this respect is the definition of the grain size. Crystals in snow have diverse shapes and do not resemble simple spherical particles such as those that occur, for instance, in fogs and water clouds. Therefore, various sizes of snow grains are measured and reported. They include, for example, the maximal and minimal dimensions of crystals, widths of branches, etc. However, as far as remote sensing is concerned, the detailed structure of snow grains cannot be accessed. Only the effective optical size of grains can be derived. How can this size

*Corresponding author. Email: alexk@iup.physik.uni-bremen.de
This paper is dedicated to the 80th birthday of Prof. A.P. Ivanov (Minsk, Belarus).

International Journal of Remote Sensing
ISSN 0143-1161 print/ISSN 1366-5901 online © 2011 Taylor & Francis
http://www.tandf.co.uk/journals
DOI: 10.1080/01431161.2011.560621

be defined? For this, one can use notions of average volume V and average projection area S of crystals. These parameters exist for any grain and, in principle, they can be measured. Therefore, we define the effective grain size (EGS) a_{ef} as the ratio of these parameters:

$$a_{ef} = \kappa \frac{V}{S}. \tag{1}$$

The parameter $\kappa = 0.75$ is introduced so that the value of a_{ef} is equal to the radius of the particles for the case of ensembles of monodispersed spheres. In the case of spherical polydispersions, a_{ef} has the simple meaning of the ratio of the third to the second moment of the size distribution. As theoretical modelling shows (Kokhanovsky and Zege 2004), the absorption cross section C_{abs} of snow grains in the region of weak light absorption is proportional to the volume of grains, independently of their shapes. Therefore, it follows that:

$$C_{abs} = A\alpha V, \tag{2}$$

where A is a constant that depends on the actual shape of a grain and also on the real part of the refractive index $m = n - i\chi$, $\alpha = 4\pi\chi/\lambda$ is the bulk ice absorption coefficient at the wavelength λ. The spectral variation of A can be neglected in the first approximation. This is due to the fact that the real part of the ice refractive index does not change considerably in the visible and near-infrared regions of the electromagnetic spectrum.

On the other hand, the extinction cross section C_{ext} is proportional to the geometrical cross section of particles S if $a_{ef} \gg \lambda$, which is always the case for snow grains in the optical range of the electromagnetic spectrum. Namely, it follows that (van de Hulst 1957):

$$C_{ext} = 2S. \tag{3}$$

Therefore, one derives for the probability of photon absorption (PPA) $\beta = C_{abs}/C_{ext}$ using equations (2) and (3):

$$\beta = \frac{A\alpha V}{2S}. \tag{4}$$

This is a very important equation. It shows that the PPA is directly proportional to the effective radius a_{ef}:

$$\beta = \frac{2}{3} A\alpha a_{ef}, \tag{5}$$

where we have used equation (1). Equation (5) holds for the polydispersions of grains with different sizes and shapes. S and V are just average values of corresponding parameters with respect to the distribution of sizes and shapes. Actually, the parameter S (but not V) is influenced by the orientation of grains. Therefore, it must also be averaged with respect to the orientation of grains. Sometimes, the following approximation is used (van de Hulst 1957, Kokhanovsky and Zege 2004):

$$< S >= \Sigma/4, \tag{6}$$

where Σ is the surface area of a grain and the brackets mean the average with respect to the random orientation of a grain. This formula is exact in the case of randomly oriented convex bodies such as spheres, ellipsoids, cylinders, etc.

The snow reflection function is governed mostly by the value of the PPA (Kokhanovsky *et al.* 2005). Therefore, there is a possibility to determine a_{ef} using optical measurements on ground, aircraft or from a satellite (Dozier *et al.* 2009). What is important here is the fact that the retrieved effective radius has a clear physical sense, which is not the case if measurements with a microscope are used, for example. Then, many averaging procedures must be performed to derive the value of a_{ef}, as determined in equation (1). To the knowledge of the authors, this procedure has actually never been done. In addition, such a measurement is difficult to make because snow is a very delicate matter, and crystals can be easily broken during the sampling procedure.

Fortunately, there is a way around this problem. The specific surface area (SSA) of snow, σ, can be measured directly. It is defined as (Domine *et al.* 2008):

$$\sigma = \frac{\bar{\Sigma}}{\rho_{\mathrm{i}} \bar{V}}, \tag{7}$$

where $\rho_{\mathrm{i}} = 0.9167$ g cm^{-3}(at 0°C) is the density of ice and $\bar{\Sigma}$, and $\bar{V}$ are the corresponding parameters averaged with respect to the size/shape distributions of the grains. The SSA gives, therefore, the surface area per mass, and it is inversely proportional to the EGS introduced above:

$$\sigma = \frac{3}{\rho_{\mathrm{i}} a_{\mathrm{ef}}}, \tag{8}$$

where we used the approximation (6). An indirect proof of this relation for snow samples was given by Matzl and Schneebeli (2006). An important issue here is that there are well established methods of the direct measurement of SSA, which can be used for the validation of the EGS defined by equation (1) as derived from satellite measurements, for example. In particular, the methane adsorption technique (Legagneux *et al.* 2002), microtomography (Schneebeli and Sokratov 2004), near-infrared photography (Matzl and Scheebeli 2006) and stereology (Matzl 2006) can be used. This means that optical measurements of a_{ef} enable the determination of SSA as well.

The retrievals of snow grain size using optical measurements have been performed by several research groups (Bourdelles and Fily 1993, Nolin and Dozier 1993, 2000, Fily *et al.* 1997, Painter *et al.* 1998, 2003, Zege *et al.* 1998, Polonsky *et al.* 1999, Nolin and Liang 2000, Hori *et al*. 2007, Stamnes *et al.* 2007, Zege *et al.* 2008, Lyapustin *et al.* 2009). In all cases a_{ef} (or the effective diameter $d = 2a_{\mathrm{ef}}$) was retrieved.

The aim of this paper is to present a fast semi-analytical snow grain size retrieval algorithm based on optical measurements. It is applied to the data from the Medium Resolution Imaging Spectrometer (MERIS), which is one of the main instruments on board the European Space Agency (ESA) Envisat platform, and also to radiances measured by the Moderate Resolution Imaging Spectroradiometer (MODIS) developed by National Aeronautics and Space Administration (NASA) and currently operating from Terra and Aqua satellite platforms.

The MERIS is composed of five cameras side by side, each equipped with a pushbroom spectrometer. These spectrometers use two-dimensional charge coupled devices (CCDs). One of the sides of the detector is oriented perpendicular to the trajectory of the satellite and simultaneously collects, through the front optics, observations for a

line of points at the Earth's surface (or in the atmosphere). The spectrometers acquire data in a large number of spectral bands, but, for technical reasons, only 16 of them are actually transmitted to the ground segment (one of which is required for low-level processing of the raw data). This instrument thus provides useful data in 15 spectral bands (412, 443, 490, 510, 560, 620, 665, 681.25, 708.75, 753.75, 760.625, 778.75, 865, 885, 900 nm), which are actually programmable in position, width and gain. In practice, these technical characteristics are kept constant most of the time to allow a large number of systematic or operational missions. The intrinsic spatial resolution of the detectors provides for samples every 300 m near nadir at the Earth's surface, and the pushbroom design avoids or minimizes the distortions (e.g. bow tie effects) typical of scanning instruments. This is known as the 'full resolution' (FR) product. The more common 'reduced resolution' (RR) products are generated by aggregating the FR data to a nominal resolution of 1200 m. The total field of view of the MERIS is 68.5° around nadir (yielding a swath width of 1150 km), which is sufficient to collect data for the entire planet every 3 days (in equatorial regions). Polar regions are visited more frequently due to the convergence of orbits. The viewing zenith angle of the MERIS changes in the range 0–40°, and so the surface bidirectional effects are minimized.

The MODIS is a key instrument aboard the Terra (Earth Observing System (EOS) AM) and Aqua (EOS PM) satellites. Terra's orbit around the Earth is timed so that it passes from north to south across the equator in the morning, while Aqua passes south to north over the equator in the afternoon. Terra MODIS and Aqua MODIS view the entire Earth's surface every 1 to 2 days, acquiring data in 36 spectral bands, or groups of wavelengths (see http://modis.gsfc.nasa.gov/about/design.php). Two bands are imaged at a nominal resolution of 250 m at nadir, with five bands at 500 m and the remaining 29 bands at 1 km. A $\pm 55°$ scanning pattern at the EOS orbit of 705 km achieves a 2330 km swath and provides global coverage every 1 to 2 days. The scan mirror assembly uses a continuously rotating double-sided scan mirror to scan $\pm 55°$ and is driven by a motor encoder built to operate at 100% duty cycle throughout the 6 year instrument design life. The optical system consists of a two-mirror off-axis afocal telescope, which directs energy to four refractive objective assemblies: one for each of the visible, near-infrared, short-wave infrared / medium-wave infrared and long-wave infrared spectral regions to cover a total spectral range of 0.4 to 14.4 μm.

The retrieval method described here is based on the fact that the reflectance in the near-infrared region (e.g. at 865 nm) depends on the PPA in snow and, therefore, on a_{ef}, as was discussed above. It shares many similarities with algorithms developed previously (e.g. Zege *et al.* 1998, 2008, Stamnes *et al.* 2007, Tedesco and Kokhanovsky 2007, Lyapustin *et al.* 2009). However, it also has some distinctive features mostly related to cloud screening and the look-up-table construction. The paper is structured as follows. In §2, we introduce the optical model of snow. Then, we study the sensitivity of spectral reflectance to the EGS in §3. The algorithm description and validation are given in §4.

2. Optical model of snow

2.1 *Theory*

The most important part of any inverse problem solution is the formulation of the forward model. How do we present snow for the purposes of the modelling of light propagation and reflection? The direct way is to introduce a great number of ice grains

of various shapes and sizes in contact and then run a Monte Carlo method specifying Fresnel reflection and transmission laws at the boundaries of grains and also absorption of photons inside the grains (Peltoniemi 2007). However, this method is AQ3
quite slow and cannot be used for the fast inverse problem solution. Therefore, we 160
pose the following question. Is it possible to use a simple model of a semi-infinite ice cloud for snow reflectance modelling? Surprisingly, as comparisons with *in situ* measurements show, this is really the case (at least in the first approximation and especially for dry snow deposited on flat surfaces). It follows that due to large sizes of particles and also due to their irregular shapes, close-packed effects do not have pronounced 165
effects as far as snow reflectance is concerned (Kokhanovsky 1998). This has also been confirmed using direct Monte Carlo ray-tracing simulations of the snow bidirectional reflection function (Peltoniemi 2007), although some small changes like snow darkening for larger snow densities were found at some geometries and wavelength). Due to this, we can directly transfer well-known techniques developed in cloud remote sens- 170
ing (Kokhanovsky 2006) to the problem of grain sizing in snow. The first issue that AQ3
we confront here is the shape of grains. How do we specify it? Several possibilities can be followed in this respect. They are

- assumption of spherical grains;
- assumed size distribution for a given particle model; and 175
- assumed size distribution for a linear superposition of different models of grains (e.g. plates and cylinders).

Actually, the retrieved grain size will depend on the assumption on the shape. This problem was not solved in cloud remote sensing, and remains the largest source of uncertainty in the results of optical sizing for ice clouds in general. The assumption of 180
spherical particles is not very realistic and must be discarded (Tanikawa *et al.* 2006, Xie *et al.* 2006). Important properties of the model to be used are (1) to give asymmetry parameters close to measured *in situ* parameters; (2) to give results similar to those reported in the ground measurements of snow angular reflectance; and (3) to be as simple as possible. To meet all three criteria specified above, we have used the model 185
of fractal grains in our previous work (Kokhanovsky and Zege 2004, Kokhanovsky *et al.* 2005). A real-life example of fractals is ice crystals freezing on a glass window. The asymmetry parameter g for the model of fractal grains is equal to 0.76 in the visible region, which is similar to values of g reported from *in situ* measurements in ice clouds (Garrett *et al.* 2001). In particular, the mean value of g measured using airborne 190
instrumentation for clouds saturated with respect to ice is 0.74 ± 0.03.

The fractal model of ice crystals was first introduced by Macke *et al.* (1996), and it is quite simple conceptually. It is based on the second generation of Koch fractals. The model is built as follows:

- the initial tetrahedron is taken (the 0th generation fractal); 195
- the smaller tetrahedrons are added to each plane of the particle (the first generation fractal, see figure 10 in Macke *et al.* (1996)); and
- the procedure is repeated at smaller triangles, leading to particles of higher generations.

As a matter of fact, we do not use, in this work, the deterministic fractal crystals 200
described above. Instead, the randomized Koch fractals of the second generation are used. A distorted Koch fractal is achieved by adding random displacements of the particle edges to the standard procedure of fractal generation. The degree of distortion

is defined by the maximum displacement length divided by the lengths of the crystal segments. This was equal to 0.2 for the simulations used in this paper. Interestingly, the phase function of randomized fractal grains is almost identical to the phase function of a stochastically deformed ice sphere with large deformation parameters (Macke *et al.* 1996, Muinonen *et al.* 1996). The only differences occur for scattering angles smaller than 30° where the Koch fractal provides some broad halos produced by the distorted tetrahedral structure. These halos are of no importance for the reflected light simulations. Therefore, we may state that irregularly shaped particles produce some robust light scattering pattern that is almost not sensitive to the actual details of the crystal shape distribution. The randomized hexagonal crystals and fractal particles also have similar angular scattering patterns (see figure 1). This is the reason behind our approach, where we use just one shape of grains to simulate the snow reflectance. Generally, the influence of particular shapes of particles on the reflectance could be quite dramatic, however. This was shown, in particular, by Xie *et al.* (2006). AQ14

We also do not use the polydispersion of fractal crystals and limit our investigation by the assumption that all crystals have the same size. This is due to the fact that the phase functions of large particles, such as irregular snow grains, do not depend on their actual dimension in the geometrical optics domain (Kokhanovsky 2006) in the visible region (outside of the forward peak). There is some dependence of the phase function on EGS in the near-infrared region due to absorption processes inside the crystals. However, corresponding effects can be neglected in the first approximation. Yet another supporting point is the fact that for retrievals, we use the fractal crystal phase function to get the reflection function in the visible region and we correct for absorption effects using notions of the asymmetry parameter g and the PPA in the framework of asymptotic radiative-transfer (RT) theory (Kokhanovsky and Zege 2004).

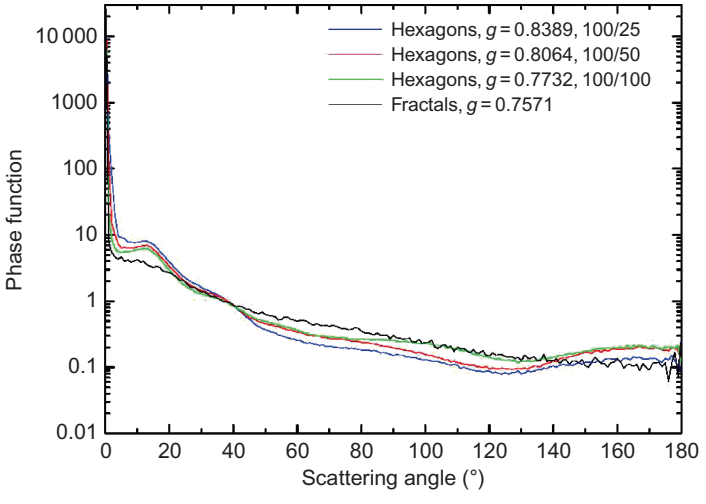

COLOUR FIGURE

Figure 1. Dependence of the phase function on the shape of particles. The following shapes were considered: hexagons with length to diameter ratios equal to 100/25, 100/50, 100/100 and fractal particles (Macke *et al.* 1996) at 550 nm wavelength. The diameter is defined as the distance between opposite sides of the hexagon. For all particles, the surface was assumed to be rough in the calculations. The asymmetry parameter g is given for each curve.

It is assumed that the snow is very deep, and therefore, the snow optical thickness does not enter our calculations. The PPA is determined as (Kokhanovsky and Nauss 2005):

$$\beta = \beta_\infty(1 - \exp(-\alpha\ell)). \tag{9}$$

This formula was obtained fitting geometrical optics results derived using the Monte Carlo code described by Macke *et al.* (1996). The value of β_∞ corresponds to the limiting case of an ice crystal that absorbs all radiation penetrated inside the particle ($\alpha\ell \to \infty$). It can be calculated using the model of spherical particles because total reflection from an impenetrable sphere and a randomly oriented non-spherical convex particle coincides (van de Hulst 1957). It follows that $\beta_\infty = 0.47$ at $n = 1.31$ (for ice). The particle absorption length (PAL) ℓ is proportional to a_{ef} (Kokhanovsky and Nauss 2005):

$$\ell = Ka_{\text{ef}}, \tag{10}$$

with the parameter K depending on the shape of particles. For weakly absorbing particles, it follows from equations (9) and (10) that:

$$\beta = \alpha\beta_\infty Ka_{\text{ef}} \tag{11}$$

and, therefore (see equation (5)),

$$K = \frac{2A}{3\beta_\infty}. \tag{12}$$

We found using geometrical optics Monte Carlo simulations and fitting procedure implemented in Origin that $K = 2.63$ for fractals.

This completes the description of the model as far as the local optical characteristics of snow are concerned (phase function, single scattering albedo $\omega_0 = 1 - \beta$ and their relationship to the size of particles).

The snow spectral and angular reflectance can be calculated solving the standard RT equation (Chandrasekhar 1960) for specified values of ω_0 and the phase function. In principle, any RT code (Lenoble 1985) can be used for this purpose. The software package SCIATRAN (Rozanov *et al.* 2005) was used in this work. In §2.2, we validate our model using ground measurements of snow reflectance under the assumption of snow vertical and horizontal homogeneity. The effects of snow roughness (e.g. sastrugi) are neglected.

2.2 *Validation of the model*

Because of the complexity of the problem and the many approximations used, it is of importance to validate the model introduced above using measurements. This will actually show how accurate we are in the selection of the phase function, for instance. For this, we have used measurements of the snow reflection function performed on lake ice in Hokkaido, Japan. For complete validation of the model, the value of a_{ef} needs to be known. However, simultaneous measurements of this parameter and snow reflectance have not been performed. Therefore, only partial validation of the model is

Table 1. Derived spectral single scattering albedo of snow (ω_0) and the corresponding measured reflection function (R) at the nadir observation, solar zenith angle, SZA=54° and relative azimuth angle, RAA = 90°.

$\lambda(\mu m)$	ω_0	R (0°, 54°, 90°)
0.55	1.0	0.917
1.05	0.9958	0.692
1.24	0.9850	0.506
1.64	0.8650	0.141
2.21	0.8938	0.174

possible. In particular, we derive the albedo of single scattering from measurements (at nadir observation and a relative azimuthal angle (RAA) of 90°, see table 1), and then we use this value of single scattering albedo in our RT simulations with SCIATRAN for the phase function of fractal grains shown in figure 1. The results of such a comparison are shown in figure 2. They confirm that the selected model is capable of describing the spectral and angular dependence of snow reflectance measured *in situ*. Generally, the theoretical curves are within errors of measurements at viewing zenith angles (VZAs) smaller than 40°. Generally, the VZA is below 40° for MERIS observations. The reflectance is more anisotropic in the near-infrared region compared to the visible region. The value of the single scattering albedo at 0.55 μm was not retrieved because it is very close to the one for pure snow located at the site. Therefore, we just plotted numerical results at $\omega_0 = 1$. This confirms that our model works both in the visible and near-infrared regions. Note that the performance of the model is worse at oblique VZAs and RAA = 0. The reflection function in the visible region is essentially flat (close to the Lambertian surface assumption) at RAA = 90°. This follows both from the theory and experiment.

Some deviations of the theory and experiment come from the experimental errors related to the shadowing of the sample by the instrument and also by the fact that the snow area under study was somewhat different for different viewing azimuthal angles.

The model is also capable of describing the hyperspectral snow reflectance. This was tested using the snow reflectance measurements in the Swiss Alps (Davos Dorf, 46.49° N, 9.51° E, 3 March 2004 (11:59–12:47)) performed with a GER3700 instrument mounted on a Field Goniometer System (Sandmeier and Itten 1999). The system is capable of measuring the snow bidirectional reflectance function. A detailed description of the measurement system and the results derived are provided by Odermatt *et al.* (2005). An example of comparisons is shown in figure 3, where we compare measurements and SCIATRAN calculations. It follows that SCIATRAN is also capable of describing hyperspectral measurements. There is a discrepancy at 1.6 μm, which does not appear in figure 2. The cause of this discrepancy could be the variation of snow properties along the vertical, which is not accounted for in the model. As a matter of fact, the value of a_{ef} varies with the height in snow and the use of the same radius at different wavelengths with a different penetration depth into snow (as was done in figure 3) is not justified (especially in the near-infrared region, where the reflectance is sensitive just to the snow grains at the top). This problem does not exist for the results shown in figure 2 because, for each wavelength, the value of ω_0 (and not just the single EGS for all wavelengths as in figure 3) was determined separately, and this value most probably corresponds to different depths in a vertically inhomogeneous snow layer.

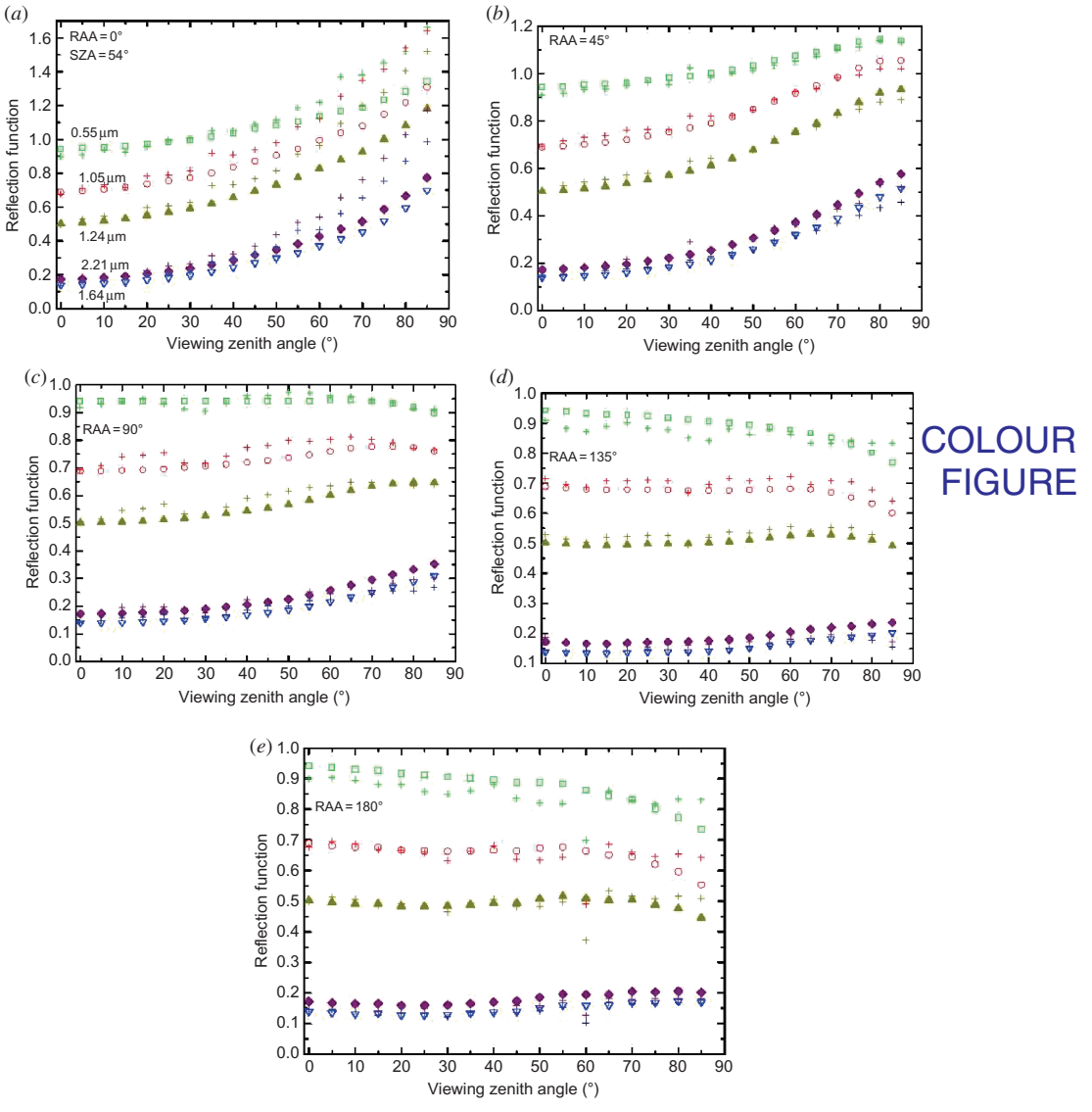

COLOUR FIGURE

Figure 2. Comparison of the measurements (crosses) and SCIATRAN (other symbols) calculations at several wavelengths. Measurements have been performed at Bihoro (Hokkaido, Japan) at 11:30 local time on 9 February 2001. The solar zenith angle (SZA) is equal to 54° and results for several relative azimuth angles (RAAs) are given. The coordinates are 43°45′30.6″N, 144°10″28.8″E .

3. Sensitivity study

300

3.1 *Theory*

The radiance I over a snow field, as detected on a satellite, depends on the snow properties and also on atmospheric parameters in the propagation channel. The snow parameter of interest in this work is the snow grain size a_{ef}. The retrievals can be

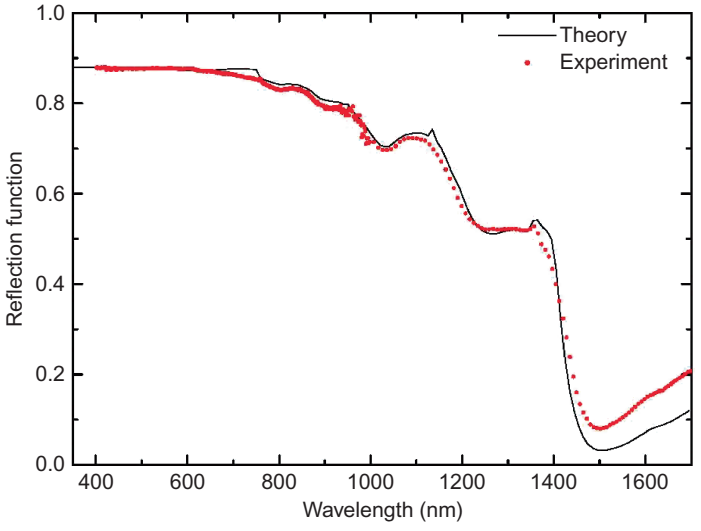

COLOUR FIGURE

Figure 3. Comparison of spectral snow reflectance measured in the Alps (Switzerland, 46.49° N, 9.51° E, 3 March 2004 (11:59–12:47)) at the solar zenith angle of 53.9°, relative azimuth angle of 45° and viewing zenith angle of 45°. SCIATRAN calculations have been performed for an ice-cloud model with the fractal ice grains (the length of the tetrahedron side $l = 290$ μm). It was assumed that snow contains soot with the volumetric concentration $c = 10^{-7}$.

affected by the concentration of pollutants (CP), c. Therefore, it is of importance to derive both parameters simultaneously. So here, we will study the sensitivity of the reflection function to the determination of both SGS and CP. AQ5

The derivatives of the reflectance $R = \pi I/\mu_0 E_0$ ($\mu_0 = \cos\vartheta_0$, $\vartheta_0$is the solar zenith angle (SZA), E_0 is the incident light irradiance) with respect to these parameters are defined as:

$$D_a = \frac{\partial R}{\partial a_{\rm ef}} \text{ and } D_c = \frac{\partial R}{\partial c}. \tag{13}$$

They help to understand if given measurements can be used to retrieve the pair ($a_{\rm ef}$, c). Clearly, derivatives depend on the viewing and illumination geometry (solar zenith angle ϑ_0, viewing zenith angle ϑ and RAA φ), the spectral channel, values of ($a_{\rm ef}$, c) and also on the atmospheric conditions (primarily, through the aerosol optical thickness (AOT), τ). So, quite generally, we can write:

$$D = f\left(\vartheta_0, \vartheta, \varphi, \lambda, a_{\rm ef}, c, \tau\right). \tag{14}$$

The task of this section is to understand how the derivatives D_a and D_c are influenced by the various parameters given in equation (14). For this, we use the software code SCIATRAN. The derivatives are calculated through the following chain of equations.

First of all the weighting function (WF) W is introduced. We define it as (e.g. in the case of WF W_a for $a_{\rm ef}$ of a homogeneous snow layer):

$$W_a = \frac{\partial R}{\partial \ln a_{\rm ef}} = a_{\rm ef} D_a. \tag{15}$$

Clearly, this is a dimensionless quantity. Then, it follows, e.g. for the reflectance function at the effective radius a_{ef}, that:

$$R\,(a_{\text{ef}}) = R(\bar{a}_{\text{ef}}) + [a_{\text{ef}} - \bar{a}_{\text{ef}}]\, W_a/\bar{a}_{\text{ef}}, \tag{16}$$

if *a priori* assumed radius $\bar{a}_{\text{ef}}$ is close to a_{ef} (so the linear approximation is valid). Clearly, if $W_a = 0$, then the reflectance is not sensitive to a_{ef}. Similar equations can be written for WFs with respect to the concentration of impurities (W_c) and also AOT (W_τ). There are different ways to calculate WFs. One possibility is the numerical calculation of ratios $M = \Delta R/\Delta(\ln x)$, where x is equal to a_{ef}, c or τ depending on the case considered. In SCIATRAN, yet another approach for the calculation of derivatives is followed. It is faster compared to the calculation of ratios M and also more accurate.

In particular, it is assumed that the variation of the reflectance δR due to the variation of the effective radius profile $\delta a_{\text{ef}}\,(z)$ inside the snow layer of thickness H can be presented in the following form:

$$\delta R\,(\lambda) = \int_0^1 w_a\,(\lambda, z)\delta a_{\text{ef}}\,(z)\,\mathrm{d}z. \tag{17}$$

Here, z is the vertical coordinate divided by the thickness of the layer H. It follows that the information on function $w_a\,(\lambda, z)$ is of great importance for understanding how changes in the profile $a_{\text{ef}}\,(z)$ influence the variation in reflectance. The WF W_a is related to $w_a\,(\lambda, z)$ via the following equation:

$$W_a\,(\lambda, z) = w_a\,(\lambda, z)\, a_{\text{ef}}(z). \tag{18}$$

Then, it follows that:

$$\delta R\,(\lambda) = \int_0^1 W_a\,(\lambda, z)\,[\delta a_{\text{ef}}\,(z)\,/a_{\text{ef}}(z)]\,\mathrm{d}z \tag{19}$$

or

$$\delta R\,(\lambda) = \sum_{k=1}^{N_k} J_a\,(\lambda, z_k)\frac{a_{\text{ef},k}\,(z) - \bar{a}_{\text{ef},k}\,(z)}{\bar{a}_{\text{ef},k}\,(z)}, \tag{20}$$

where the summation is performed for the number of layers N_k inside the snow layer specified in the input of SCIATRAN and:

$$J_a\,(\lambda, z_k) = W_a\,(\lambda, z_k)\,\Delta z_k \tag{21}$$

are corresponding Jacobians related to a sub-layer of thickness Δz_k. For a homogeneous layer, it follows that:

$$\delta R\,(\lambda) = [\delta a_{\text{ef}}/a_{\text{ef}}]\, W_a\,(\lambda, z)\,, \tag{22}$$

and we return to the same expression as written above:

$$R\,(a_{\rm ef}) = R(\bar{a}_{\rm ef}) + \Delta R = R(\bar{a}_{\rm ef}) + [a_{\rm ef} - \bar{a}_{\rm ef}]\, W_a/\bar{a}_{\rm ef}. \tag{23}$$

The WF $W_a\,(\lambda, z_k)$ contains information not only on the dependence of R on $a_{\rm ef}$ but also on the sensitivity of the reflectance to the changes in the radii of grains at different layers inside the snow.

The derivatives:

$$W_a\,(\lambda) = \sum_{k=1}^{N_k} J_a\,(\lambda, z_k) \tag{24}$$

and also the Jacobians $J_a\,(\lambda, z_k)$ are the main parameters discussed in the next section. The corresponding derivatives and Jacobians with respect to the concentration of pollutants and AOT are also considered.

As follows from equation (20), W_a in equation (24) gives the change in the reflectance (δR) if the change in the radius is equal to 100%. The technique to derive $w_a\,(\lambda, z)$ using the solution of direct and adjoint RT equations is described by Rozanov *et al.* (2007).

3.2 *Results*

The results of numerical experiments on sensitivity studies are shown in figure 4, where derivatives are plotted. All results were obtained using SCIATRAN (www.iup.physik.uni-bremen.de/~sciatran) and assuming that snow can be modelled as an ice cloud with the optical thickness 5000 at the ground level (with the fractal phase function shown in figure 1). It was assumed that snow impurities (soot) are present in the form of Rayleigh scatterers and they influence only absorption and not scattering processes in a snow layer. The PPA was modelled using equation (38) (see also equations (9) and (41)). The LOWTRAN aerosol maritime model implemented in SCIATRAN with τ (550nm) = 0.05 was used. In addition, the molecular scattering (but not absorption) has been taken into account. SCIATRAN is able to simulate satellite signals taking into account gaseous absorption. However, this was not needed for this work because only channels almost free of gaseous absorption have been selected.

It follows from figure 4 that the 1.02 and 1.24 μm channels are most suitable for grain size monitoring from space. For soot concentration retrievals, the shortest wavelength must be used (e.g. 0.443 nm). The uncertainty in the knowledge of the AOT is of importance for the soot concentration retrievals (especially for low soot contents). The atmospheric correction is less important for the grain size retrieval because the terrestrial atmosphere is generally quite transparent in the near-infrared region in polar regions.

We have also calculated the vertical profiles of corresponding Jacobians (not shown here) and found that they differ from zero only for upper layers of snow (10–20 cm in the visible region and below 1–2 cm in the near-infrared region). This means that the soot concentration can be derived only in the upper snow layer. There is no information in the visible channels for soot and dust buried at deep layers. The grain size

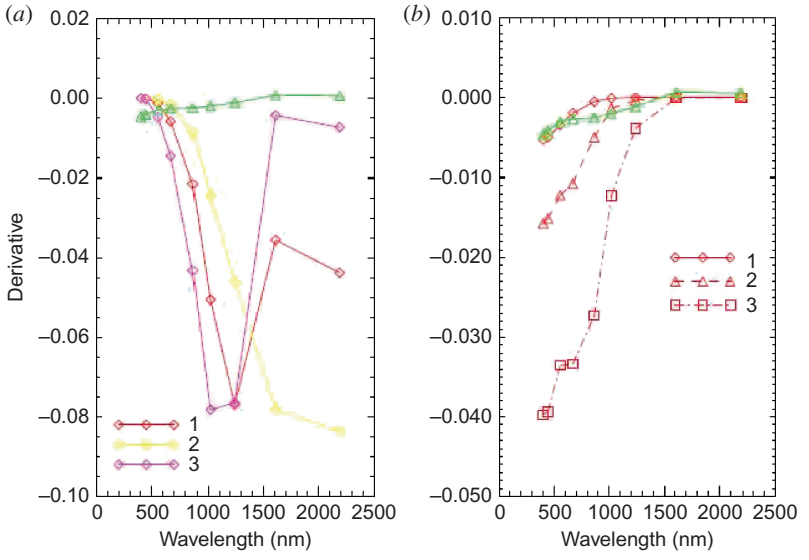

COLOUR FIGURE

Figure 4. Dependence of the derivatives: (*a*) W_a (1 – 300 μm, 2 – 50 μm, 3 – 750 μm fractal particles) and (*b*) W_c(1–$c = 10^{-8}$, 2–$c = 10^{-7}$, 3–$c = 10^{-6}$) on the wavelength. The LOWTRAN aerosol model with an aerosol optical thickness (AOT) equal to 0.05 was used. The snow geometrical thickness is equal to 1m. The concentration of soot is equal to 10^{-8} for all curves in (*a*). The 300 μm fractal particles are used for all lines in (*b*) (red colour). The green colour gives the derivative with respect to aerosol optical thickness. The solar zenith angle is equal to 60°, and the observation is at the nadir direction (viewing zenith angle is equal to 0°).

can be determined only for the upper snow layers due to low penetration of infrared radiation into snow.

4. Retrieval algorithm

The developed retrieval algorithm for the SGS determination is based on the look-up-table (LUT) approach. In particular, the Fourier components of the reflection function in the visible region (for a non-absorbing snow) are tabulated using the code developed by Mishchenko *et al.* (1999). The code solves the Ambartsumian non-linear integral equation for the harmonics $R^m(\mu, \mu_0)$ of the reflection function. These harmonics are stored in LUTs. Then, the reflection function at any relative azimuth angle is found:

$$R(\mu, \mu_0, \varphi) = R^0(\mu, \mu_0) + 2\sum_{m=1}^{M_{\max}} R^m(\mu, \mu_0)\cos(m\varphi). \tag{25}$$

Here, $\mu = \cos\vartheta$ and the value of $M_{\max}$ is chosen from the condition that the next term does not contribute more than 0.01% in the sum of equation (25). In principle, one more dimension (for a given phase function) in this LUT is needed, and this is the dimension of the single scattering albedo. Taking into account that MERIS measurements stop at the wavelength 0.9 μm and ice is only weakly absorbing in the spectral range of the MERIS (0.4–0.9 μm), we use asymptotic RT theory (Zege *et al.* 1991) for calculations of snow reflectance at absorbing wavelengths. This also simplifies the

retrieval algorithm, reducing it to analytical equations. Therefore, no minimization procedure is required, and the inverse problem can be solved analytically.

In particular, we use the following representation valid as $\omega_0 \to 1$(Zege *et al.* 1991, Kokhanovsky 2006):

$$R(\mu, \mu_0, \varphi) = R_0(\mu, \mu_0, \varphi) A^{f(\mu, \mu_0, \varphi)}, \tag{26}$$

where

$$A = \exp\left\{-4s/\sqrt{3}\right\}, s = \sqrt{\frac{1-\omega_0}{1-g\omega_0}}, f = \frac{u(\mu_0)\, u(\mu)}{R_0^{-1}(\mu, \mu_0, \varphi)} \text{ and } u(\mu) = \frac{3}{7}(1+2\mu). \tag{27}$$

Here, R_0 is the reflection function of a semi-infinite snow layer under the assumption that the single scattering albedo is equal to one. It is calculated using equation (25). For pure snow, the experimentally measured value of R_0 (e.g. at 443 nm) can be used. This speeds up the retrievals.

The only approximation compared to the exact RT calculations involved is the use of the term A^f in equation (26) to characterize light absorption by snow. We found that errors are below 6% compared to SCIATRAN calculations at the wavelengths 0.52–1.24 μm and SZA = 54° for all azimuthal angles. Namely, these short wavelengths are used here for the inverse problem solution. In the case of MERIS wavelengths 443 and 865 nm, the errors are smaller than 2% at VZAs<40°, typical for MERIS observations. This is well inside the calibration error of the MERIS. If high accuracy is not of primary concern, then an approximation for the function $R_0(\mu, \mu_0, \varphi)$ given below can be used. This speeds up retrievals and make it easier to perform various types of sensitivity studies.

The reflection function of non-absorbing snow $R_0(\mu, \mu_0, \varphi)$ can be calculated in the following approximation:

$$R_0(\mu, \mu_0, \varphi) = \frac{A + B(\mu + \mu_0) + C\mu\mu_0 + p(\theta)}{4(\mu + \mu_0)},$$

where A=1.247, B=1.186, C=5.157, $p(\theta) = 11.1\exp(-0.087\theta) + 1.1\exp(-0.014\theta)$, θ is given in degrees and defined as $\theta = a\cos(-\mu\mu_0 + ss_0\cos\varphi)$, φ is the relative azimuth, $\mu = \cos(\text{VZA})$ and $\mu_0 = \cos(\text{SZA})$. The accuracy of this approximation is better than 15% for the MERIS observation conditions (Kokhanovsky 2006).

The MERIS does not have channels above 0.9 μm and, therefore, the approximation proposed here is very relevant to the interpretation of MERIS observations over snow fields. This is due to the fact that the snow albedo (and the accuracy of the approximation) increases for shorter wavelengths. The forward model itself (e.g. the flat snow surface assumption) and also errors of atmospheric correction introduce much larger errors compared to differences between approximate and exact theories.

Equation (27) can be used for the analytical determination of ω_0 and, therefore, a_{ef} from the snow reflection function measurements. As a matter of fact, in the case of small grains and the MERIS wavelengths, an even simpler approximation can be used. This approximation follows from equation (26) as $\omega_0 \to 1$:

$$R(\mu, \mu_0, \varphi) = R_0(\mu, \mu_0, \varphi) - \frac{4s}{\sqrt{3}} u(\mu)\, u(\mu_0). \tag{28}$$

Equation (26) also enables the determination of the snow spectral albedo:

$$A(\lambda) = (R_{\text{mes}}(\lambda)/R_0)^{1/f} \tag{29}$$

from measurements of the spectral reflection function just at one observation geometry. It is assumed that the atmospheric correction has already been performed, and that the influence of the atmosphere is removed from the value of $R_{\text{mes}}(\lambda)$. The determination of the snow albedo also means that the snow reflection function $R = \pi I/\mu_0 E_0$ and the snow bidirectional reflection function BRDF $= R/\pi$ are also found simultaneously at any viewing geometry (see equation (21)). In addition, the spectral snow similarity parameter is determined (see equation (27)): AQ7

$$s(\lambda) = \frac{\sqrt{3}}{4} \ln\left[\frac{1}{A(\lambda)}\right]. \tag{30}$$

This parameter is of importance for the understanding of RT in snow.

The technique given above enables the determination of spectral characteristics $A(\lambda)$, $s(\lambda)$ and BRDF(λ) up to the wavelength 1.24 μm. We also found that the particular non-spherical grain shape assumption is not crucial for the snow albedo retrieval. In fact, different assumptions on the grain shape produce very similar values of the spectral albedo in the framework of our retrieval approach.

The single scattering albedo can be found from the expression for the similarity parameter only if the value of the asymmetry parameter is known. For dry snow, one can assume that the asymmetry parameter only weakly depends on the wavelength and one can assume that $g = 0.76$, as discussed above, independently of the wavelength (in the spectral range considered), as for fractal grains. For the wet snow, the value of g increases and the retrieval results for the single scattering albedo (but not the snow surface albedo) will be biased. Using equation (27) for s gives:

$$\omega_0(\lambda) = \frac{1 - s^2(\lambda)}{1 - g s^2(\lambda)}. \tag{31}$$

An important point is that although ω_0 will be possibly biased due to the assumption on the value of the asymmetry parameter, the spectral behaviour of ω_0 is not affected by this assumption because (for large snow grains) g is almost a spectrally neutral parameter. Moreover, because $gs^2 \to 0$ in the spectral range studied, the influence of the incorrect assumption on the value of the asymmetry parameter does not influence results for ω_0 considerably. In many applications, the PPA is needed, and not ω_0. It follows that:

$$\beta(\lambda) = \frac{(1-g)s^2(\lambda)}{1 - g s^2(\lambda)}, \tag{32}$$

and the error in $\varepsilon = 1 - g$ influences results considerably. However, again, the spectrum $\beta(\lambda)$ is not much affected by the assumption of the value of ε because it is almost a spectrally neutral parameter in the spectral range considered.

The shape of particles must be assumed for the retrieval of the grain effective size from the value of the PPA given by equation (32) using the results presented above (see equations (9) and (10)). The value of the single scattering albedo in the near-infrared

region ($\lambda \geq 0.8 - 1.0$ μm) is almost independent of the snow pollution. Therefore, it is proposed to find PAL and also a_{ef} in the near-infrared region (e.g. 1.02 μm or at 0.865 μm (MERIS / Advance Along-Track Scanning Radiometer (AATSR))). Then, the retrieved value of the grain effective radius can be used to determine the fraction of the PPA related to the pollution (in the visible region). Actually, if one chooses the wavelength of 443 nm, then the imaginary part of the refractive index of ice is so small ($\sim 10^{-10}$) that the whole absorption can be attributed to impurities and not to snow grains.

At the wavelength 0.865 μm, there is a chance (for highly polluted snow only) that the signal is contaminated by the contribution of pollutants. This contamination effect can be easily accounted for by slightly modifying the algorithm described above.

Namely, we use the fact that it is possible to write for channels 1 (0.443 μm) and 2 (0.865 μm) in the approximation under study:

$$R_1 = R_0 \exp(-\gamma\sqrt{\beta_1}) \tag{33}$$

and

$$R_2 = R_0 \exp(-\gamma\sqrt{\beta_2}), \tag{34}$$

where indices 1 and 2 signify the channel, and:

$$\gamma = \frac{4f}{\sqrt{3(1 - g\omega_0)}}. \tag{35}$$

We will neglect the difference of ω_0 from 1.0 in the dominator of equation (35).

Here, we assume that there is some light absorption by snow, even in the visible region (e.g. due to soot). The value of the PPA can be written as:

$$\beta = \frac{N_{\rm i} C_{\rm abs,i} + N_{\rm s} C_{\rm abs,s}}{N_{\rm i} C_{\rm ext,i} + N_{\rm s} C_{\rm ext,s}}. \tag{36}$$

Here,

$$N_{\rm s} = \frac{c_{\rm s}}{\bar{V}_{\rm s}} \tag{37}$$

is the number concentration of soot particles, $\bar{V}_{\rm s}$ is their average volume, $c_{\rm s}$ is the volumetric concentration of soot (the fraction of volume filled by soot), $C_{\rm abs,s}$ is the average absorption cross section of soot particles, $C_{\rm ext,s}$ is the average extinction cross section of soot particles. Parameters with the index 'i' have the same meaning as described above, except that they are for ice.

We will neglect the contribution of soot to the general light extinction in snow. Then, it follows that:

$$\beta = \beta_{\rm i} + \beta_{\rm s}, \tag{38}$$

where $\beta_{\rm i} = \frac{C_{\rm abs,i}}{C_{\rm ext,i}}$ is given by equation (9) and

$$\beta_s = \frac{V_i c_s C_{abs,s}}{V_s c_i C_{ext,i}}. \tag{39}$$

The average extinction cross section of the ice grains $C_{ext,i}$ can be estimated as follows (see equations (3) and (6)):

$$C_{ext,i} = \frac{\bar{\Sigma}_i}{2}. \tag{40}$$

Here $\bar{\Sigma}_i$ is the average surface area of grains. Taking into account that $C_{ext,i}/\bar{V}_i = 1.5\, a_{ef}^{-1}$ in this approximation and also assuming that $C_{abs,s}/\bar{V}_s = B\alpha_s$, which is true in the Rayleigh domain for small soot particles ($B = 0.84$ at the soot refractive index $n = 1.75$ (van de Hulst 1957), $\alpha_s = 4\pi\chi_s/\lambda$, $\chi_s = 0.46$), we derive:

$$\beta_s = \frac{2}{3} B c \alpha_s a_{ef}, \tag{41}$$

where:

$$c = c_s/c_i \tag{42}$$

is the relative soot concentration.

The mass absorption coefficient of soot $\sigma_{abs} = C_{abs}/\rho_s \bar{V}_s$ is equal to $B\alpha_s/\rho_s$ in the considered approximation. Here, ρ_s is the soot density. Assuming that $B = 0.84$, $\chi_s = 0.46$, $\lambda = 443$ nm and $\rho_s = 1$ g cm^{-3}, one derives $\sigma_{abs} = 8.4$ g m^{-2}, which is close to the modern estimates of this parameter (7.5 ± 1.2 m^2 g^{-1}(Bond and Bergstrom 2006, Flanner *et al.* 2007).

Therefore, we can write:

$$R_1 = R_0 \exp\left[-\gamma\sqrt{\frac{2}{3} B\alpha_{s,1} c a_{ef}}\right] \tag{43}$$

and

$$R_2 = R_0 \exp(-\gamma\sqrt{\beta_{i,2} + \frac{2}{3} B\alpha_{s,2} c a_{ef}}). \tag{44}$$

Here, we have neglected light absorption by ice at the first wavelength. These two equations can be used to find both the size of ice crystals and the concentration of pollutants. It follows from the first equation for $X = ca_{ef}$ that:

$$X = \frac{3}{2B\gamma^2\alpha_{s,1}} \ln^2 r_1 \tag{45}$$

and, therefore,

$$\beta_2 = \frac{\ln^2 r_2}{\gamma^2} - \frac{2}{3} BX\alpha_{s,2}, \tag{46}$$

where X is determined from equation (45). Here, we have introduced the normalized reflectance: $r_{\rm i} \equiv R_{\rm i}/R_0$. The EGS can be found from equations (9) and (10):

$$a_{\rm ef} = K\alpha_{\rm i,2}^{-1} \ln\left[\frac{\beta_\infty}{\beta_\infty - \beta_2}\right]. \tag{47}$$

Then, the concentration of soot is determined as $c = X/a_{\rm ef}$. In practice, one measures the concentration of soot as the fraction of soot mass in a given mass of snow $c_{\rm f} = c_{\rm s}\rho_{\rm s}/c_{\rm i}\rho_{\rm i}$, where $\rho_{\rm s}$ is the density of soot and $\rho_{\rm i}$ is the density of ice. Therefore, for the transformation of the satellite-derived c to the ground measured values of $c_{\rm f}$, one must use the multiplier $\eta = \rho_{\rm s}/\rho_{\rm i}$:

$$c_{\rm f} = \eta c. \tag{48}$$

We will assume that $\eta \equiv 1$in this study. It is known that $\rho_{\rm i} = 0.917$ g cm^{-3}. The density of soot depends on its structure. It varies in the range $1 - 2$ g cm^{-3}. The assumption of $\eta \equiv 1$ is consistent with the lower limit of this variability.

For the MODIS, the channel at 1.24 μm is available in addition to the 0.865 μm channel. The Global Imager (GLI) of the Japan Aerospace Exploration (JAXA), which is currently not in operation, had several channels relevant to snow remote sensing (e.g. located at 0.865, 1.05 and 1.24 μm). The applications of the asymptotic RT theory for these sensors were given by Zege *et al.* (1998, 2008), Polonsky *et al.* (1999), Tedesco and Kokhanovsky (2007) and Lyapustin *et al.* (2009).

Generally, the wavelength 1.24 μm is the best for retrievals in the case of homogeneous snow because then heavy pollution does not influence the results of the grain size retrieval (therefore, one can put X=0 in the expression for β_2 and derive the following simplified equation: $\beta_2 = \gamma^{-2}\ln^2 r_2$, which can be used in conjunction with equation (47) for the retrievals of $a_{\rm ef}$). For vertically inhomogeneous snow, this wavelength brings information only from the top of the layer and may not be consistent with grains at deeper layers seen by the 443 nm wavelength used for the snow pollution retrieval. Even if measurements at 865 nm are used, there is quite a large mismatch in the volume of snow sensed using the 443 nm and 865 nm wavelengths. We found (not shown here) that the Jacobians for the soot concentration (at 443 nm) approach zero at the distance of 20 cm from the top layer and the values of the Jacobians for the EGS vanish already at 2–5 cm, depending on the wavelength. Therefore, a possible soot layer deposited at, say, 5 cm from the snow top will influence the signal in the visible region, but not at 865 nm. This makes the application of a dual-wavelength algorithm not possible in this case, and one should use the single channel algorithm based on equations (47) and (46) at $X = 0$.

It follows in the case of multiple pollutants that:

$$\beta = \frac{N_{\rm i}C_{\rm abs,i} + \sum\limits_{\alpha=1}^{M} N_\alpha C_{{\rm abs},\alpha}}{N_{\rm i}C_{\rm ext,i} + \sum\limits_{\alpha=1}^{M} N_\alpha C_{{\rm ext},\alpha}}. \tag{49}$$

Here,

$$N_\alpha = \frac{c_\alpha}{V_\alpha} \tag{50}$$

is the number concentration of α-pollutant particles, V_α is their average volume, c_α is the volumetric concentration of α-pollutant (the fraction of volume filled by this particular pollutant), $C_{\mathrm{abs},\alpha}$ is the absorption cross section of the α-pollutant and $C_{\mathrm{ext},\alpha}$ is the extinction cross section of the α-pollutant. If dust is present in large quantities, the second term in the dominator of equation for β cannot be ignored, and such parameters as the size of dust grains and also their concentration must be determined, along with the parameters for soot. The necessity for such retrievals occurs only on rare occasions (heavy dust pollution events), and we will not explore this opportunity in the present work.

5. The validation of the algorithm using MODIS data and simultaneous ground measurements of grain size

The validation of the algorithm has been performed using MODIS top-of-atmosphere spectral reflectances collocated (temporally and spatially) with ground measurements of snow properties in Hokkaido, Japan. Characterization of the validation sites is presented in table 2. The experimentally measured grain sizes are given in table 3, and maps of the reflectances are shown in figure 5. The retrievals have been performed for the snow field in the centre of the image (red colour in figure 5(*a*)). The algorithm developed by us (called FORCE) can be used for arbitrary channels. The channels of 460/865 nm and also the single channel at 1240 nm have been used in the retrievals. A map of the EGS retrieved using channel at 1240 nm is shown in figure 6. It follows that the EGS is around 0.1 mm for the area studied. AQ8

Corresponding MODIS data (500 m spatial resolution) are presented in table 4. The results of the inter-comparison of snow grain size retrievals (using channels 460 and 1240 nm) and ground measurements are given in figure 7. In the case of satellite measurements, the EGS is defined as the ratio of the average volume of particles to their average surface area multiplied by 3. Therefore, the EGS coincides with the radius of particles in the case of monodispersed spheres. The EGS measured on the ground is denoted by r, and it is equal to the half of the snow dendrite width (or a narrower portion of a broken ice crystal (Aoki *et al.* 2007)). Clearly, r and a_{ef} are different quantities. However, it is expected that they correlate. Indeed such a correlation exists,

Table 2. Characterization of validation sites. *Measurements have been performed at several sites close to the indicated location. The range of the viewing zenith angles (VZAs) of the MODIS and the solar zenith angle range (SZA) are also given.

Site	Saroma*	Abashiri	Nakashibetsu
Latitude	44°07′09″N	43°58′15″N	43°29′56″N
Longitude	143°55′46″E	144°11′37″E	144°42′50″E
Underlying surface	Lagoon ice	Lake ice	Farmland
Date	05 February 2001 24 February 2002 26 February 2002	15 March 2004	22 March 2004 24 March 2004
SZA range (°)	56.1–61.7	47.1–47.6	43.1–49.4
VZA range (°)	1.5–22.5	12.9–20.8	0.1–54.9
Snow type	Dry	Wet	Wet, crust

Table 3. The grain size r measured on the ground at various sites.

Case number	Date	Site	r (mm), deep layers	r (mm), upper layer
1	05 February 2001	Saroma site C	0.309	0.095
2	24 February 2002	Saroma site C	0.284	0.060
3	24 February 2002	Saroma site 2	0.120	0.125
4	24 February 2002	Saroma site 2'	0.169	0.75
5	24 February 2002	Saroma site 6	0.280	0.125
6	24 February 2002	Saroma site 5	0.194	0.150
7	24 February 2002	Saroma site 7	0.366	0.163
8	24 February 2002	Saroma site 8	0.335	0.150
9	24 February 2002	Saroma site 3	0.438	0.188
10	24 February 2002	Saroma site 4	0.114	0.100
11	26 February 2002	Saroma site 8	0.296	0.275
12	26 February 2002	Saroma site 5	0.218	0.073
13	26 February 2002	Saroma site 4	0.111	0.105
14	26 February 2002	Saroma site C	0.271	0.098
15	26 February 2002	Saroma site 2	0.71	0.110
16	15 March 2004	Abashiri	0.361	0.300
17	15 March 2004	Abashiri	0.361	0.300
18	22 March 2004	Nakashibetsu	0.411	0.375
19	22 March 2004	Nakashibetsu	0.589	0.250
20	24 March 2004	Nakashibetsu	0.432	0.500
21	24 March 2004	Nakashibetsu	0.523	0.325

as illustrated in figure 7 (the correlation coefficient is equal to 0.57), if channels 460 and 865 nm are used both for the grains at the surface and also in deeper snow layers. As expected, the correlation increases (to 0.71), if the channel at 1240 nm is used instead of 865 nm (see figure 8). The results of retrievals by FORCE give similar results as those derived by using an independent EGS retrieval algorithm developed at JAXA (see figure 9 (Stamnes *et al.* 2007)).

The reason for a quite low correlation is further explained in figure 10, where we plot the MODIS reflectance at 1240 nm as a function of the EGS measured on the ground. According to the theory, all points in figure 10 must lie on one line ($R \approx R_0 - K\sqrt{a_{\rm ef}}$, where R is the measured reflectance, R_0 is the reflection function of non-absorbing snow, and K is the coefficient of proportionality). As follows from figure 10, this is not the case. Generally, R decreases with the EGS, but this is just a general trend, with many exceptions, as shown in figure 10. This points out to the difficulty of correct grain size determination on the ground. One possibility to avoid this problem with ground measurements is to measure the EGS using light reflectance at the ground (e.g. at 1240 nm) and not optical microscopy. Then the problems related to the manual determination of the grain size are not relevant anymore. This enables the inter-comparison of ground and satellite-derived sizes of crystals, which still may differ due to imperfect atmospheric correction and a poor sampling of satellite pixels by ground measurements.

6. Application of the algorithm to MERIS data

6.1 *Cloud screening*

The task of this section is to apply the algorithm to MERIS data. For the determination of clear-sky snow pixels, we use the differential snow index determined as:

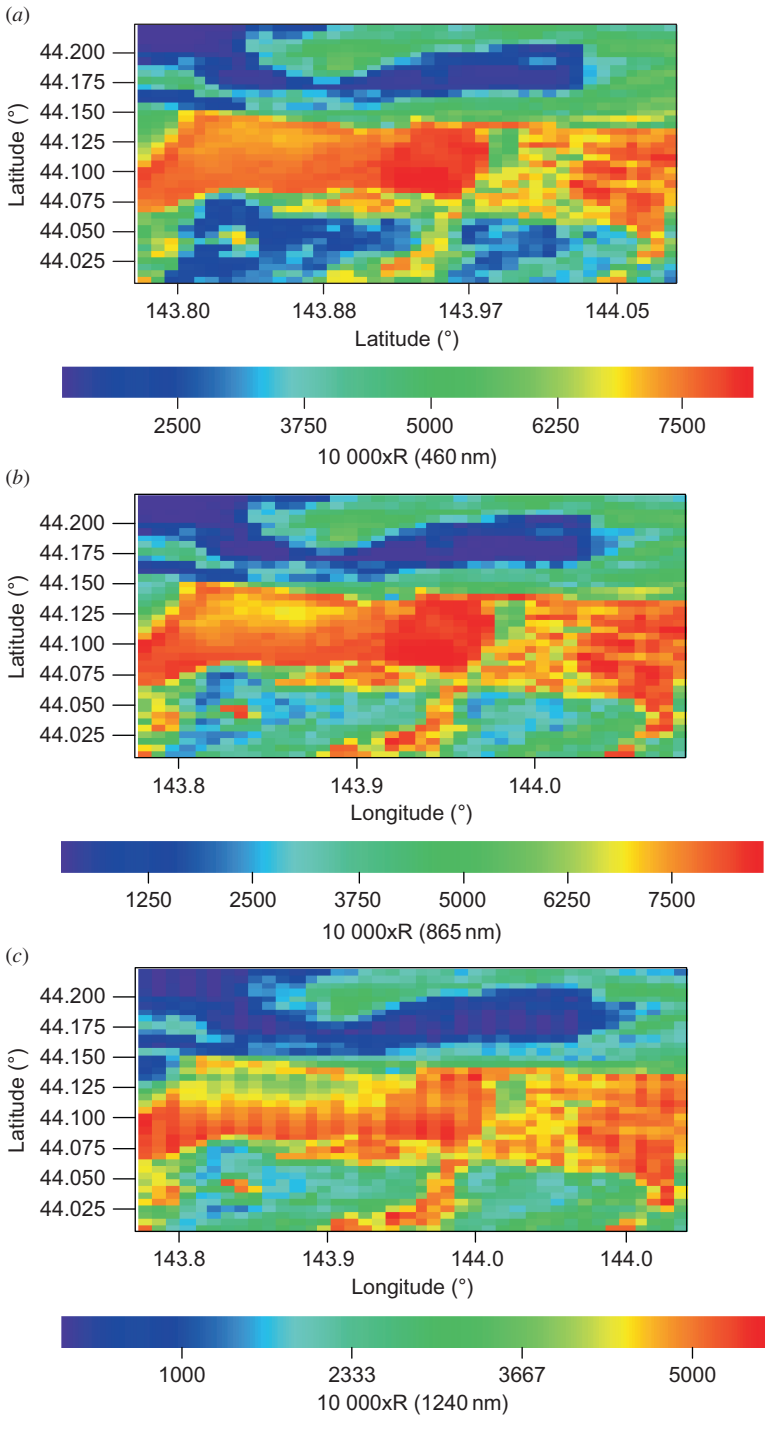

COLOUR FIGURE

Figure 5. Maps of MODIS reflectance at: (*a*) 460 nm ($\times 10^4$), (*b*) 865 nm ($\times 10^4$) and (*c*) 1240 nm ($\times 10^4$).

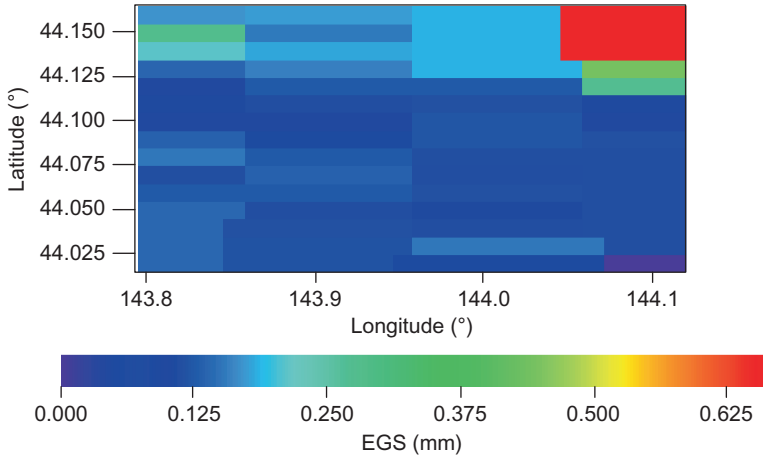

COLOUR FIGURE

Figure 6. Retrieved grain size (wavelengths 460 and 1240 nm were used in the retrievals).

Table 4. MODIS satellite data for locations and times given in table 3. The reflectance R shown in this table at a given wavelength (645, 865, 555, 1240 and 1640 nm) is defined as $10000\,\pi I/\mu_0 E_0$. Values of viewing zenith angle (VZA), viewing azimuth angle (VAZ), solar zenith angle (SZA) and solar azimuth angle (SAZ) are also given (in $^\circ \times 100$). Each line in table 4 coincides with a corresponding line in table 3.

R(645)	R(865)	R(460)	R(555)	R(1240)	R(1640)	VZA	VAZ	SZA	SAZ
7145	7780	7088	6791	4117	1097	145	10 521	6167	16 319
7933	8395	7974	7656	4911	1441	173	11 059	5606	15 873
7662	8093	7805	7484	4734	1344	176	11 421	5607	15 874
7646	8105	7747	7426	4824	1353	166	11 417	5606	15 875
7402	7679	7592	7269	4415	1281	182	11 012	5606	15 872
7390	7749	7512	7181	4440	1310	191	10 970	5607	15 870
7791	8208	7874	7557	4720	1338	165	11 111	5605	15 874
7763	8177	7859	7538	4809	1371	156	11 169	5605	15 876
7839	8319	8149	7843	5126	1572	166	10 867	5605	15 874
8100	8555	8135	7834	5239	1722	162	10 485	5604	15 873
7250	7689	7416	7018	3912	925	2215	9889	5618	15 510
6754	7176	6979	6542	3625	878	2251	9885	5620	15 504
7491	7889	7620	7214	4085	993	2234	10 047	5618	15 507
7154	7682	7362	6934	3942	925	2233	9887	5619	15 507
7178	7688	7343	6943	3930	871	2233	9911	5620	15 508
7038	6940	6778	6745	2741	766	2084	−7758	4763	16 134
7203	6721	6877	6897	2144	506	1295	7854	4707	−16 474
6837	6819	6329	6156	2755	767	3359	−7548	4392	16 385
6994	6572	6806	6722	2242	461	12	1417	4446	−16 035
6512	6226	6073	6107	1777	318	1532	−7872	4382	15 949
6773	6234	6325	6400	1441	281	2102	7786	4306	−16 421

$$\varsigma = \frac{R\,(865\text{ nm}) - R(885\text{ nm})}{R\,(865\text{ nm}) + R(885\text{ nm})}, \tag{51}$$

and also some criteria for $\Re = R(865\text{ nm})$. As a matter of fact, for clouds, reflectance increases with the wavelength in the spectral range 865–885 nm and ς is often takes

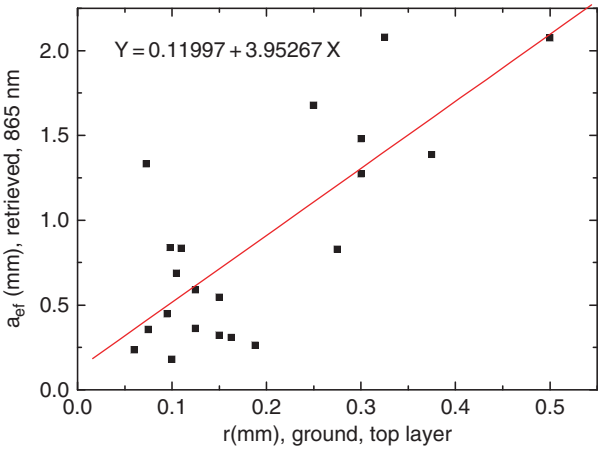

COLOUR FIGURE

Figure 7. Correlation of satellite-derived and ground-measured grain size. The correlation coefficient is equal to 0.57.

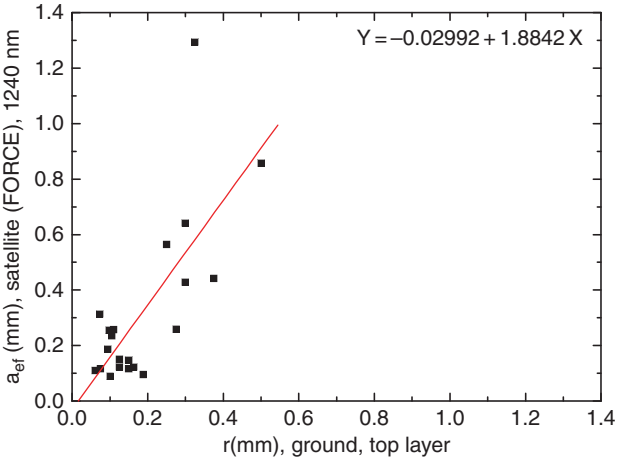

COLOUR FIGURE

Figure 8. Correlation of satellite-derived and ground-measured grain size. The correlation coefficient is equal to 0.73 (0.81, if one single point (around 1.3 mm) is removed).

negative values. For snow and ice, ς is positive. The following assumptions have been introduced for the selection of clear-sky snow pixels:

- $\varsigma > 0.01$;
- $\Re$ is in the range 0.75–1.0;
- $|\varepsilon| < 0.001$, $\varepsilon = 1 - \frac{\bar{\Re}_{\text{local}}}{\Re_{\text{middle}}}$, $\bar{\Re}_{\text{local}}$ is the average of $\Re$ for the seven neighbouring MERIS pixels, $\Re_{\text{middle}}$ is the value of reflectance for the pixel located in the middle of the seven selected pixels; and
- $\Re$ at any point in the particular area Σ does not differ by more than $\pm 10\%$ from the reflectance averaged for the scene (in the averaging procedure, only pixels that pass the conditions given above are used). The size of the area Σ depends on the

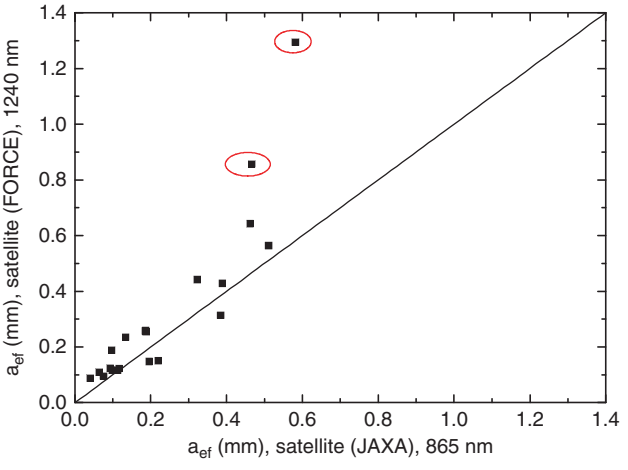

COLOUR FIGURE

Figure 9. Correlation of satellite-derived grain sizes. The correlation is very good, except for the two points circled.

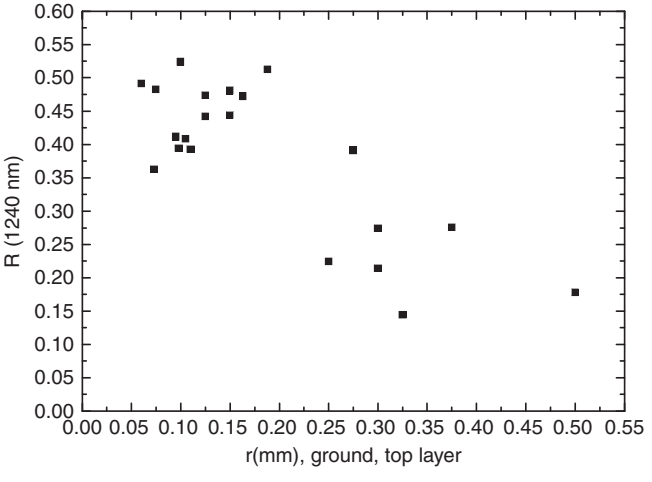

Figure 10. Dependence of satellite reflectance at 1240 nm on ground-measured grain size.

snow field under consideration. Clearly, this condition can be applied only to the case of homogeneous snow fields (Antarctica, Greenland).

In addition, if thermal infrared measurements are available (like for MODIS), the following additional conditions are used to identify clear pixels over snow (Ackerman *et al.* 2006, Kokhanovsky and Shreier 2008):

- brightness temperature BT (11 μm) >250 K;
- R (3.7 μm) $\geq$ 0.05; and
- temporal variability of R (3.7 μm) is checked. Several orbits are analysed to see if the reflectance at 3.7 μm at a given location changes with time. For clear-snow pixels, it is assumed that this change is small.

The reflectance at 3.7 μm is calculated as follows (Spagenberg *et al.* 2001): AQ3

$$R\,(3.7\ \mu\text{m}) = \frac{(B - B^{+})e}{\mu_0 S(3.7\ \mu\text{m}) - B^{+}e}, \tag{52}$$

where B is the measured brightness temperature at 3.7 μm, B^{+} is the 3.7 μm BT derived by using a Planck distribution for the measurement at 11 μm, $e = 0.964$ is the clear-snow emittance at 3.7 μm and S is the solar constant.

6.2 *Results of retrievals*

A MERIS browse image of the snow field under clear sky in Greenland is shown in figure 11. The corresponding maps of reflectances at 443 nm and 865 nm are given in figure 12. Many clouds are present in the region. They are screened out effectively by the cloud-screening algorithm described above. The retrieved grain size is shown in figure 13. The average EGS is around 0.2 mm for the whole scene and 0.15 mm for the left part of the scene, Unfortunately, *in situ* data for EGS at this location during the satellite measurements are not available to us. AQ9

We show the results of the retrieved concentration of pollutants in figure 14 (in ng g^{-1}). The concentrations are very low, as one might expect for the Arctic. Generally, as follows from the sensitivity studies given above, the accurate determination of soot concentration from a satellite is difficult in the Arctic due to the low concentration of pollutants there. Although, as can be seen from figure 14, the magnitude of c is determined correctly in the case presented here.

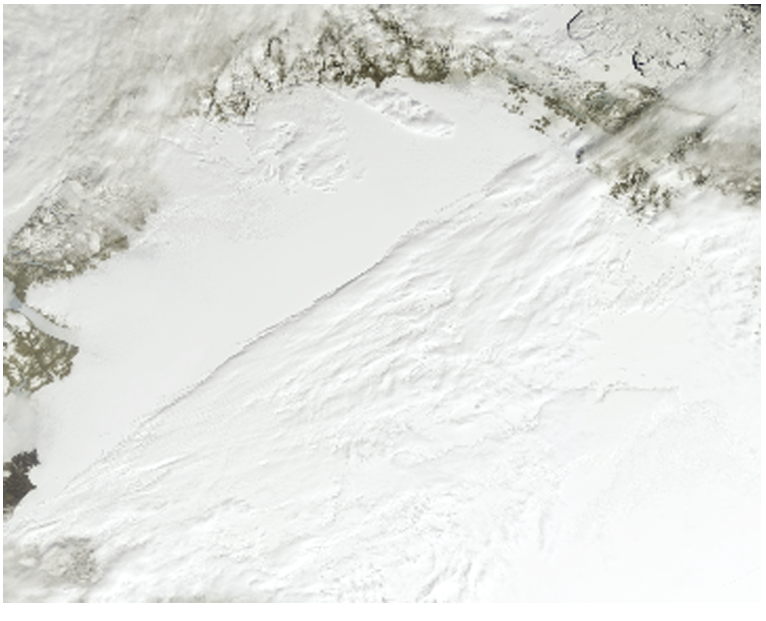

COLOUR FIGURE

Figure 11. A MERIS browse image of the scene analysed.

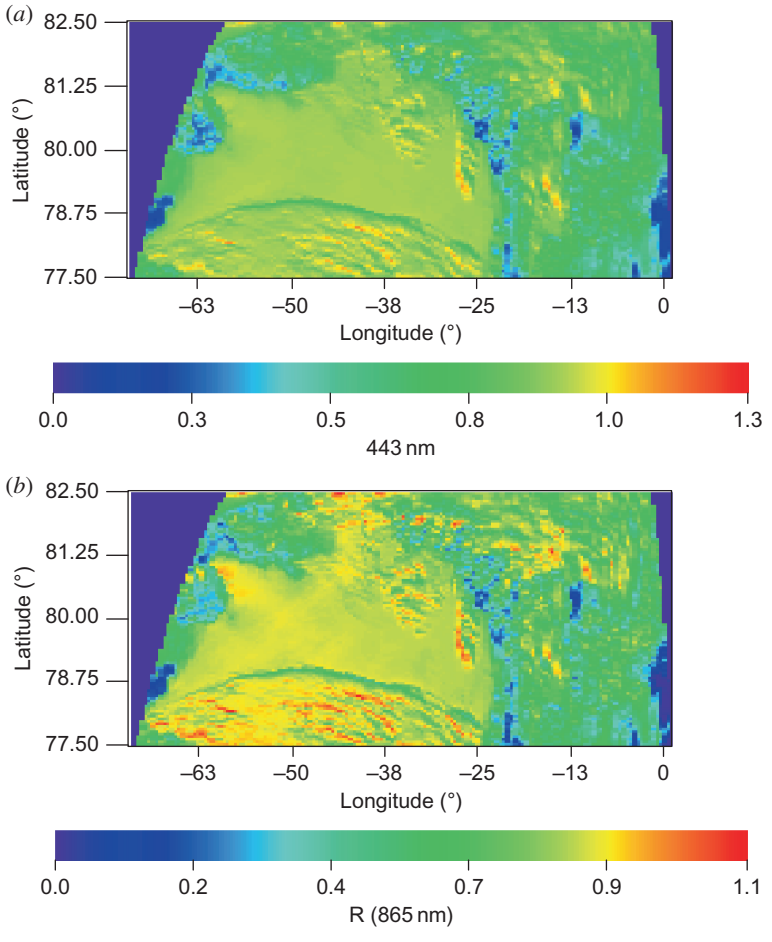

COLOUR FIGURE

Figure 12. Maps of reflectances at: (*a*) 443 nm and (*b*) 865 nm for the browse image shown in figure 11. The cloud in the lower part of the image corresponds to the cloud in the right-hand corner on figure 11.

7. Conclusions

In this work, we have proposed and validated a new snow grain size retrieval algorithm FORCE. The correlation coefficient between satellite and ground measurements of the EGS was in the range 0.6–0.7. The small values of the correlation coefficient could be due to the different definitions of sizes in the ground and satellite measurements. We have also proposed techniques for cloud screening and atmospheric correction of satellite images over snow. The algorithm needs to be improved in the future. The current version of the algorithm was implemented in the European Space Agency software package BEAM and is free for use by the remote-sensing community.

Several simplifications have been used in the retrievals. In particular, it was assumed that the snow was vertically homogeneous. In reality, snow has a layered structure, as discussed by Colbeck (1991). The layering arises from a sequence of storms, reworking of the snow surface into a distinctive horizon, which is subsequently buried, or the generation of certain types of horizons within the snow profile. The sequence of these

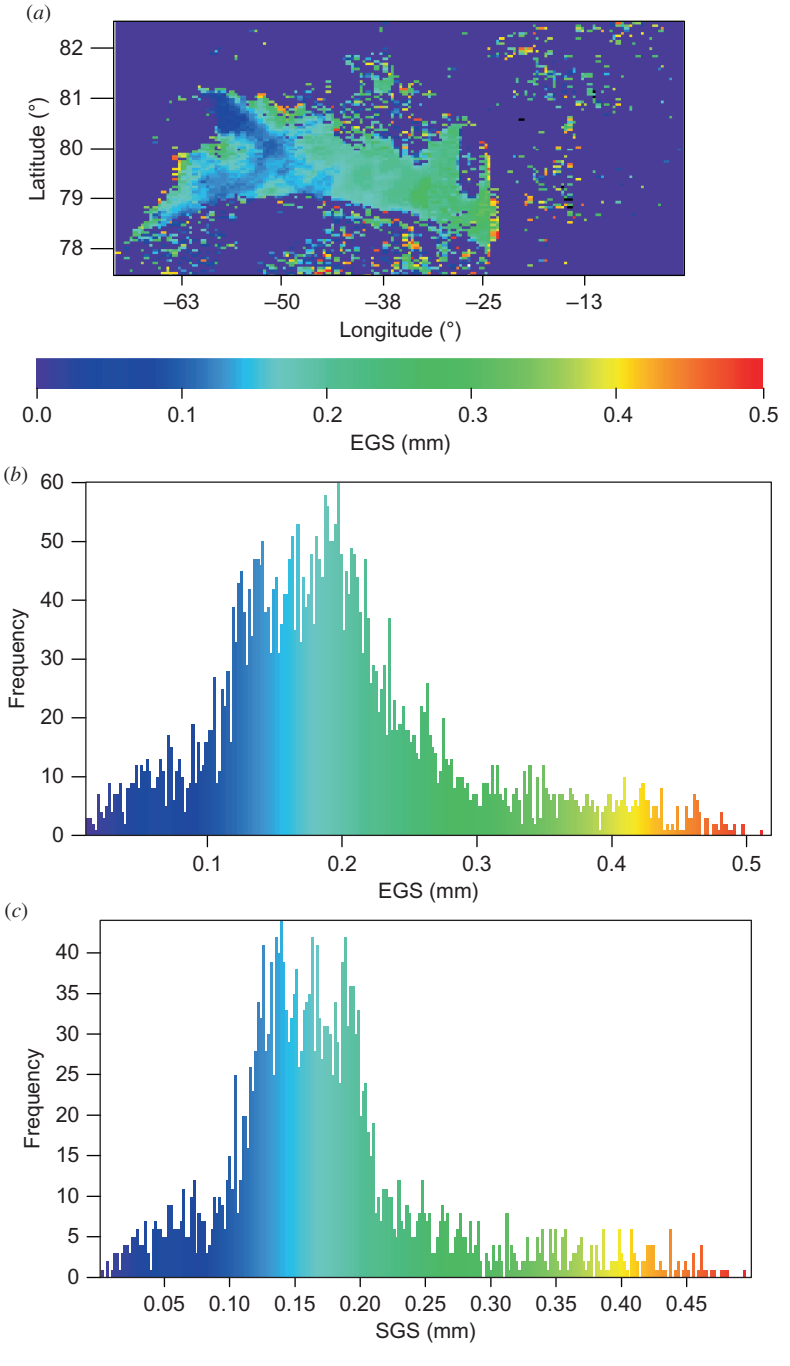

COLOUR FIGURE

Figure 13. (*a*) Retrieved snow grain size and (*b*) its histogram (the lower panel corresponds to retrievals in the left part of the image, where the sizes are somewhat smaller).

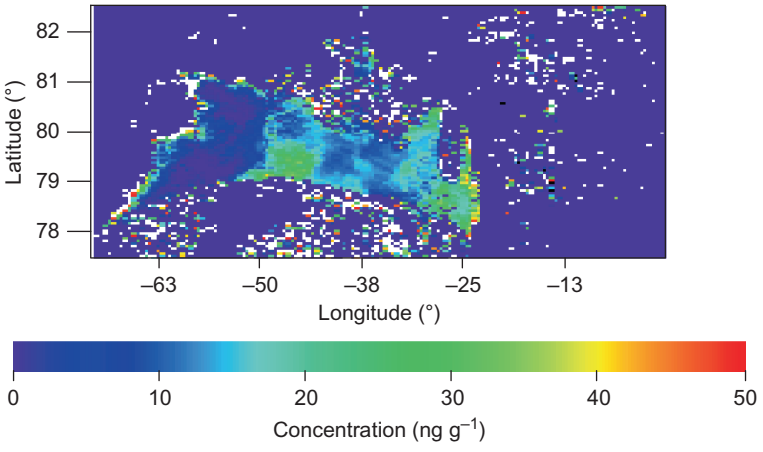

Figure 14. Retrieved concentration of pollutants.

buried layers is not only unique from year to year and highly variable with location, but each layer also evolves as the snowy season progresses (Colbeck 1982, 1983). Dust and soot can be deposited in such layers and then covered by fresh snow. Vertically homogeneous snow is assumed in standard retrieval algorithms, and the pollutant content derived will be that of an entire snow column, which does not correspond to reality. Moreover, in retrievals, one needs to assume the refractive index of the pollutants. The refractive index is considerably different for dust and soot. In addition, the absorption and scattering cross sections of soot and dust particles are considerably different. Therefore, wrong *a priori* assumptions on the type of pollutants (soot, dust, red algae on the surface of snow) prevent correct retrievals of the concentration of pollutants. In principle, the type of pollutants can be distinguished from spectral measurements of the snow reflectance because, for example, dust and soot have different spectral bulk absorption coefficients (e.g. red and grey colours). However, this is possible only for thin covers of fresh snow over dirty snow or the freshly polluted snow cases.

In addition, it follows that the structure of snow and also the shapes/sizes of crystals are very different from the top to the bottom of the snow layer. This peculiarity is also not accounted in the forward model. The snow grain size has been retrieved using infrared measurements. However, it is a well-known fact that the imaginary part of the refractive index of ice changes with the wavelength. This means that light with different wavelengths will penetrate to different depths. Therefore, the use of multiple wavelengths, in principle, can reveal the vertical distribution of the snow grains (Li *et al.* 2001, Zhou *et al.* 2003). Using one wavelength retrieval, only one size for a given depth is retrieved. Importantly, the snow penetration depth is not fixed for a given wavelength, but it also depends on the grain size itself. Generally, it is lower for larger wavelengths. Therefore, it is of importance to report at which wavelength the retrievals have been performed. If pollution is not uniformly distributed in snow, but rather contained in distinct layers (e.g. dust), then one cannot ignore light scattering by pollutants. Then, both absorption and scattering effects by pollutants must be considered. Usually in retrievals of the EGS, the pollution is assessed assuming homogeneous distribution of the snow layer. If pollution is in the layer well below the snow surface (see figure 36), plays no role in the EGS retrieval, but it can play some role if AQ10

pollutants are close to the surface and retrievals are done at a short wavelength (e.g. 865 nm) and grains are small.

Yet another problem is the possible existence of an ice layer on the top of the snow (crust). Crust snow is what happens when the surface of powder snow melts and then re-freezes. This action leaves a layer of ice on top of the snow that can make retrievals of the snow grain size underneath difficult if this thin ice layer is not accounted for in the retrieval process properly. When the air temperature becomes warmer than the freezing point, the snow starts to melt, and its water content becomes very high. With this, the delicate snow crystals change into large grains of ice, and slush is formed. Slush is basically snow that is starting to melt and thus becomes further wet. Satellite retrievals of snow grain size for very wet snow such as slush are not possible.

The RT models used extensively in the snow optics assume that snow has no structure on the surfaces. For satellite ground scenes (e.g. 1 km^2), the horizontal in homogeneity of snow (e.g. sastrugi) may influence the snow BRDF and, therefore, the retrieved snow grain size considerably (Warren *et al.* 1998). It was found using Monte Carlo calculations (Zuravleva and Kokhanovsky 2011) that generally, the reflectance decreases if sastrugi is present, and that the decrease could be of the order of 5–30%, depending on the PPA. It is smaller for smaller PPA. Patches of vegetation penetrating through snow or trees make retrievals impossible or difficult. Therefore, it is of importance to make not only cloud screening, but also only 100% snow-covered ground scenes (without forest and vegetation) must be used in retrievals of the grain size, snow albedo and the concentration of snow pollutants. This is due to the fact that there is a limitation with respect to the complexity of the forward model, which can be used in the retrieval process. Although there are some reports on the retrieval of sub-pixel snow properties (e.g. Painter *et al.* 1998, 2003, 2009), retrieval of snow properties in mountainous regions is also a problem. Then, effects of shadowing are evident and three-dimensional RT models are needed with known topography and illumination conditions at a given location.

The retrievals of grain sizes for polluted cases (both for polluted snow and atmosphere) can cause problems, if the channel at 865 nm is used for retrievals. This is due to the fact that the signal at 865 nm can be influenced by pollution (Painter *et al.* 2007), and this influence is difficult to assess *a priori.* For instance, there is a problem of soot possibly present in the atmosphere and in the snow. For larger wavelengths, the influence of pollution is reduced considerably. Dozier *et al.* (2009) reported that there are cases where the pollution (e.g. dust) influences snow reflectance at all wavelengths in the visible and near-infrared regions (up to $\lambda = 1.4\ \mu m$). The retrieval of the pollution level also depends on the type of pollution (Warren and Wiscombe 1980, Warren 1982, Painter and Dozier 2004, Painter *et al.* 2007). The uncertainty in the imaginary part of the ice refractive index in the visible region (Warren and Brandt 2008) can also play a role.

As noted by Peltoniemi (2007), snow becomes less reflective at larger densities of snow. The RT theory can be applied at very low densities (actually not possible for snow on the ground) only and, therefore, this darkening will be interpreted as the presence of pollutants – although, in fact, the snow is fresh and clean. In particular, this could be the reason behind the observed reduction of fresh snow reflectance in the visible region compared to RT simulations (e.g. figure 5 in Dozier *et al.* (2009)).

The RT model described above is valid for dry snow only. During the melting season, water can accumulate in the snow. Then, the model must be changed taking into account the snow darkening due to the presence of liquid water in the snow.

Both modifications of snow absorption and scattering are important. The snow grains become more spherical and grow in size. Clusters are formed (Colbeck 1979). The presence of liquid films between grains reduces the scattering and also leads to more extended in the forward direction phase functions. This will definitely bias retrievals if it is not accounted for in the retrieval procedure. The issues highlighted above are the subject of our ongoing research on forward and inverse models in snow optics.

Acknowledgements

This work was supported by the ESA Project Snow_Radiance and also by JAXA S-GLI Project (Japan). Alexander Kokhanovsky thanks Andreas Macke and Michael Mishchenko for providing their codes that were used in this study, and Eleonora Zege for a number of discussions on snow optics. We thank ESA and NASA for providing satellite data.

References

Ackerman, S., Strabala, K., Menzel, P., Frey, R., Moeller, C., Gumley, L., Baum, B., Wetzel, S., Seemann, S. and Zhang, H., 2006, Discriminating clear sky from cloud with MODIS algorithm theoretical basis document (MOD35). Available online at http://modis.gsfc.nasa.gov/data/atbd/atbd_mod06.pdf.

Aoki, T., Hori, M., Motoyoshi, H., Tanikawa, T., Hachikubo, A., Sugiura, K., Yasunari,T.J., Storvold,R., Eide, H.A., Stamnes, K., Li, W., Nieke, J., Nakajima,Y. and Takahashi, F., 2007, ADEOS-II/GLI snow/ice products – part II: validation results using GLI and MODIS data. *Remote Sensing of Environment*, **111**, pp. 274–290.

Bond, T.C. and Bergstrom, R.W., 2006, Light absorption by carbonaceous particles: an investigative review. *Aerosol Science and Technology*, **40**, pp. 27–67.

Bourdelles, B. and Fily, M., 1993, Snow grain-size determination from Landsat imagery over Terre Adelie, Antarctica. *Annals Glaciology*, **17**, pp. 86–92.

Chandrasekhar, S., 1960, *Radiative Transfer* (New York, NY: Dover).

Colbeck, S.C., 1979, Grain cluster in wet snow. *Journal of Colloid and Interface Sciences*, **72**, pp. 371–384.

Colbeck, S.C., 1982, An overview of seasonal snow metamorphism. *Review of Geophysics and Space Physics*, **20**, pp. 45–61.

Colbeck, S.C., 1983, Theory of metamorphism of dry snow. *Journal of Geophysical Research*, **88**, pp. 5475–5482.

Colbeck, S.C., 1991, The layered character of snow covers. *Reviews of Geophysics*, **29**, pp. 81–96.

Domine F., Albert, M., Huthwelker,T., Jacobi, H.-W., Kokhanovsky, A., Lehning, M., Picard, G. and Simpson, W.R., 2008, Snow physics as relevant to snow photochemistry. *Atmospheric Chemistry and Physics*, **8**, pp. 171–208.

Dozier, J., 1987, Recent research in snow hydrology. *Reviews of Geophysics*, **25**, pp. 153–161.

Dozier, J. and Painter, T.H., 2004, Multispectral and hyperspectral remote sensing of alpine snow properties. *Annual Review of Earth and Planetary Sciences*, **32**, pp. 465–494.

Dozier, J., Green, R.O., Nolin, A.W. and Painter, T.H., 2009, Interpretation of snow properties from imaging spectrometry. *Remote Sensing of Environment*, **113**, pp. S25–S37.

Fily, M., Bourdelles, B., Dedieu J.P. and Sergent, C., 1997, Comparison of *in situ* and Landsat Thematic Mapper derived snow grain characteristics in the Alps. *Remote Sensing of Environment*, **59**, pp. 452–460.

Flanner, M.G., Zender, C.S., Randerson, J.T. and Rasch, P.J., 2007, Present-day climate forcing and response from black carbon in snow. *Journal of Geophysical Research*, **112**, p. D11202, doi:10.1029/2006JD008003.

GARRET, T.J., HOBBS, P.V. and GERBER, H., 2001, Shortwave, single scattering properties of Arctic ice clouds. *Journal of Geophysical Research*, **106**, pp. 15 555–15 172.

HANSEN, J. and NAZARENKO, L., 2004, Soot climate forcing via snow and ice albedos. *Proceedings of National Academy of Sciences of USA*, **101**, pp. 423–428. AQ12

HORI, M., AOKI, T., STAMNES, K. and LI,W., 2007, ADEOS-II/GLI snow/ice products – part III: retrieved results. *Remote Sensing of Environment*, **111**, pp. 291–336.

KOKHANOVSKY, A.A., 1998, On light scattering in random media with large densely packed particles. *Journal of Geophysical Research*, **103**, pp. 6089–6096.

KOKHANOVSKY, A.A. and NAUSS, T., 2005, Satellite based retrieval of ice cloud properties using semianalytical algorithm. *Journal of Geophysical Research*, **D110**, p. D19206, doi: 10.1029/2004JD005744.

KOKHANOVSKY, A.A. and SCHREIER, M., 2008, The determination of snow albedo using combined AATSR and MERIS observations. In *Proceedings of 2nd MERIS/(A)AATSR Workshop*, 22–26 Septembber 2008, Frascati, Italy, (ESA SP-666, November 2008).

KOKHANOVSKY, A.A. and ZEGE, E.P., 2004, Scattering optics of snow. *Applied Optics*, **43**, pp. 1589–1602.

KOKHANOVSKY, A.A., AOKI, T., HACHIKUBO, A., HORI, M. and ZEGE, E.P., 2007, Reflective properties of natural snow: approximate asymptotic theory versus *in situ* measurements. *IEEE Transactions on Geosciences and Remote Sensing*, **43**, pp. 1529–1535. AQ12

LEGAGNEUX, L., CABANES, A. and DOMINE, F., 2002, Measurement of the specific surface area of 176 snow samples using methane adsorption at 77 K. *Journal of Geophysical Research*, **107**, p. 4335, doi: 10.1029/2001JD001016.

LENOBLE, J., 1985, *Radiative Transfer in Scattering and Absorbing Atmospheres: Standard Computational Procedures* (Hampton, VA: Deepak).

LI, W., STAMNES, K., CHEN, B. and XIONG, X., 2001, Snow grain size retrieved from near-infrared radiances at multiple wavelengths. *Geophysical Research Letters*, **28**, pp. 1699–1702, doi: 10.1029/2000GL011641.

LYAPUSTIN, A., TEDESCO, M., WANG, Y., AOKI, T., HORI, M. and KOKHANOVSKY, A., 2009, Retrieval of snow grain size over Greenland from MODIS. *Remote Sensing of Environment*, **113**, pp. 1976–1987.

MACKE, A., MUELLER, J. and RASCHKE, E., 1996, Single scattering properties of atmospheric ice crystals. *Journal of Atmospheric Science*, **53**, pp. 2813–2825.

MATZL, M., 2006, Quantifying the stratigraphy of snow profiles. PhD thesis, Swiss Federal Institute of Technology, Zürich, Switzerland.

MATZL, M. and SCHNEEBELI,M., 2006, Measuring specific surface area of snow by near-infrared photography. *Journal of Glaciology*, **52**, pp. 558–564.

MISHCHENKO, M.I., DLUGACH, J.M., YANOVITSKIJ, E.G. and ZAKHAROVA, N.T., 1999, Bidirectional reflectance of flat, optically thick particulate layers: an efficient radiative transfer solution and applications to snow and soil surfaces. *Journal of Quantitative Spectroscopy and Radiative Transfer*, **63**, pp. 409–432.

MUINONEN, K., NUSIAINEN, T., FAST, P., LUMME, K. and PELTONIEMI, J.I., 1996, Light scattering by Gaussian random particles: ray optics approximation. *Journal of Quantitative Spectroscopy and Radiative Transfer*, **55**, pp. 577–601.

NOLIN, A.W. and DOZIER, J., 1993, Estimating snow grain size using AVIRIS data. *Remote Sensing of Environment*, **44**, pp. 231–238.

NOLIN, A.W. and DOZIER, J., 2000, A hyperspectral method for remotely sensing the grain size of snow. *Remote Sensing of Environment*, **74**, pp. 207–216.

NOLIN, A.W. and LIANG, S., 2000, Progress in bidirectional reflectance modeling and applications for surface particulate media: snow and soils. *Remote Sensing Reviews*, **18**, pp. 307–342.

ODERMATT, D., SCHLÄPFER, D., LEHNING, M., SCHWIKOWSKI, M., KNEUBÜHLER, M. and ITTEN, I.K., 2005, Seasonal study of directional reflectance properties of snow. *EARSeL eProceedings*, **4**, pp. 203–214.

PAINTER, T.H. and DOZIER, J., 2004, Measurements of the hemispherical-directional reflectance of snow at fine spectral and angular resolutions. *Journal of Geophysical Research*, **109**, D18115, doi: 10.1029/2003JD004458.

PAINTER, T.H., ROBERTS, D.A., GREEN, R.O. and DOZIER, J., 1998, The effect of grain size on spectral mixture analysis of snow-covered area from AVIRIS data. *Remote Sensing of Environment*, **65**, pp. 320–332.

PAINTER, T.H., DOZIER, J., ROBERTS, D.A., DAVIS, R.E. and GREENE, R.O., 2003, Retrieval of subpixel snow-covered area and grain size from imaging spectrometer data. *Remote Sensing of Environment*, **85**, pp. 64–77.

PAINTER, T.H., BARRETT, A.P., LANDRY, C.C., NEFF, J.C., CASSIDY, M.P., LAWRENCE, C.R., MCBRIDE, K.E. and FARMER, G.L., 2007, Impact of disturbed desert soils on duration of mountain snow cover. *Geophysical Research Letters*, **34**, p. L12502, doi: 10.1029/2007GL030284.

PAINTER, T.H., RITTGER, K., MCKENZIE, C., SLAUGHTER, P., DAVIS, R.E. and DOZIER, J., 2009, Retrieval of subpixel snow covered area, grain size and albedo from MODIS. *Remote Sensing of Environment*, **113**, pp. 868–879.

POLONSKY, I.N., ZEGE, E.P., KOKHANOVSKY, A.A., KATSEV, I.L. and PRIKHACH, A.S., 1999, The retrieval of the effective radius of snow grains and control of snow pollution with GLI data. In *Geoscience and Remote Sensing Symposium, IGARSS '99 Proceedings, IEEE 1999 International*, 28 June−2 July 1999, vol. 2, pp. 1071–1073, doi: 10.1109/IGARSS.1999.774536.

ROZANOV, A.A., ROZANOV, V.V., BUCHWITZ, M., KOKHANOVSKY, A.A. and BURROWS, J.P., 2005, SCIATRAN 2.0 – a new radiative transfer model for geophysical applications in the 175–2400 nm spectral range. *Advances in Space Research*, **36**, pp. 1015–1019.

ROZANOV, V.V., ROZANOV, A.V. and KOKHANOVSKY, A.A., 2007, Derivatives of the radiation field and their application to the solution of inverse problems. In *Light Scattering Reviews*, A.A. Kokhanovsky (Ed.), vol. 2, p.205–265.

SANDMEIER, S.R. and ITTEN, K.I., 1999, A Field Goniometer System (FIGOS) for acquisition of hyperspectral BRDF data. *IEEE Transactions on Geoscience and Remote Sensing*, **37**, pp. 978–986.

SCHNEEBELI, M. and SOKRATOV, S.A., 2004, Tomography of temperature gradient metamorphism of snow and associated changes in heat conductivity. *Hydrological Processes*, **18**, pp. 3655–3665.

STAMNES, K., LI, W., EIDE, H., AOKI, T., HORI, M. and STORVOLD, R., 2007, ADEOS-II/GLI snow/ice products – part I: scientific basis. *Remote Sensing of Environment*, **111**, pp. 258–273.

TANIKAWA, T., AOKI, T., HORI, M., HACHIKUBO, A. and ANIYA, M., 2006, Snow bidirectional reflectance model using nonspherical snow particles and its validation with field measurements. *EARSeL Proceedings*, **5**, pp. 137–145.

TEDESCO, M. and KOKHANOVSKY, A.A., 2007, The semi-analytical snow retrieval algorithm and its application to MODIS data. *Remote Sensing of Environment*, **110**, pp. 317–331.

TOMASI, C., VITALE, V. and LUPI, A., 2007, Aerosols in polar regions: a historical overview based on optical depth and *in situ* observations. *Journal of Geophysical Research*, **112**, p. D16205, doi: 10.1029/2007JD008432.

VAN DE HULST, H.C., 1957, *Light Scattering by Small Particles* (New York, NY: Wiley).

WARREN, S.G., 1982, Optical properties of snow. *Reviews of Geophysics*, **20**, pp. 67–89.

WARREN, S.G., 1984, Optical constants of ice from the ultraviolet to the microwave. *Applied Optics*, **23**, pp. 1206–1225.

WARREN, S.G. and WISCOMBE, W.J., 1980, A model for the spectral albedo of snow. II: snow containing atmospheric aerosols. *Journal of Atmospheric Sciences*, **37**, pp. 2734–2733.

WARREN, S.G., BRANDT, R.E. and HINTON, P., 1998, Effects of surface roughness on bidirectional reflectance of Antarctic snow. *Journal of Geophysical Research*, **103**, pp. 25 789–25 807.

AQ12

WARREN, S.G. and BRANDT, R.E., 2008, Optical constants of ice from the ultraviolet to the microwave: a revised compilation. *Journal of Geophysical Research*, **113**, p. D14220, doi: 10.1029/2007JD009744.

XIE, Y., YANG, P., GAO, B.-C., KATTAWAR, G.W. and MISHCHENKO, M.I., 2006, Effect of ice crystal shape and effective size on snow bidirectional reflectance. *Journal of Quantitative Spectroscopy and Radiative Transfer*, **100**, pp. 457–469.

ZEGE, E.P., IVANOV, A.P. and KATSEV, I.L., 1991, *Image Transfer Through a Scattering Medium* (Berlin, Germany: Springer).

ZEGE, E.P., KOKHANOVSKY, A.A., KATSEV, I.L., POLONSKY, I.N. and PRIKHACH, A.S., 1998, The retrieval of the effective radius of snow grains and control of snow pollution with GLI data. In *Proceedings of Conference on Light Scattering by Nonspherical Particles: Theory, Measurements and Applications*, M.I. Mishchenko, L.D. Travis and J.W. Hovenier (Eds), pp. 288–290 (Boston, MA: American Meteorological Society).

ZEGE, E.P., KATSEV, I.L., MALINKA, A., PRIKHACH, A.S. and POLONSKY, I.N., 2008, New algorithm to retrieve the effective snow grain size and pollution amount from satellite data. *Annals of Glaciology*, **49**, pp. 139–144.

ZHOU, X., LI, S. and STAMNES, K., 2003, Effects of vertical inhomogeneity on snow spectral albedo and its implications for remote sensing of snow. *Journal of Geophysical Research*, **108**, p. 4738, doi: 10.1029/2003JD003859.

ZURAVLEVA, T.B. and KOKHANOVSKY, A.A., 2011, Influence of surface roughness on the reflective properties of snow. *Journal of Quantitative Spectroscopy Radiative Transfer*, submitted. **AQ13**